INSTITUTE OF TECHNOLOGY

AIR UNIVERSITY

UNITED STATES AIR FORCE

SCHOOL OF ENGINEERING

THESIS

WRIGHT-PATTERSON AIR FORCE BASE, OHIO

AF-WP-B-SEP 60 5M

ANALOG SIMULATION AND ANALYSIS OF A NON-LINEAR SELF-ADAPTIVE FLIGHT CONTROL SYSTEM

THESIS

Presented to the Faculty of the School of Engineering of
Institute of Technology
Air University
in Partial Fulfillment of the
Requirements for the Degree of
Master of Science

By
Thomas J. Deegan
Major USAF
Graduate Astronautics

August 1961

AF-WP-O-DEC 61 21

Preface

This report is a result of my study of the General Electric Self-Adaptive Control (GESAC) system. I have attempted in this report to provide a departure point for studies of this or similar systems by outlining a method for optimizing the analog simulation. In addition, the gain-changing dynamics of the non-linear frequency sensor were considered, and the effects of noise on system operation were observed.

I would like to take this opportunity to express my appreciation to the many people who have helped make this report possible. My thanks go to Major John H. Blakelock, my Faculty Thesis Adviser, and to Lt Thomas J. Hayes, my Thesis Sponsor, both of whom have been a source of advice and guidance throughout the course of this study. Also, I would like to thank Mr. Richard Boucher of the General Electric Company, who was of great assistance in my quest for an understanding of the basic principles of operation of the GESAC system.

I would also like to express my appreciation to Major Joseph B. Evans who worked tirelessly to help iron out the many difficulties that arose in the process of this simulation and to Lt Eugene Henry, who, while on military leave from the University of Notre Dame, made

important contributions to the design of the frequency-sensor simulation. My thanks also go to Capt Stewart B. Herndon, who generously devoted time from his thesis work on the digital computer (IBM 1620) to check the validity of my root locus data.

Finally, I would like to thank my wife who, in addition to maintaining a houseful of eight children, was of great help in the preparation of this report.

Thomas J. Deegan

Contents

Contents

List of Figures

List of Figures

List of Tables

Symbols and Definitions

All the symbols used in this report are defined below, except for those which are defined in the text.

Dimensional	Units
Distance	feet
Time	seconds
Angle	radians (unless otherwise stated)
Force	pounds

Aerodynamic	Notation
m	mass
h	altitude
ρ	air density
c	wing chord
q_i	dynamic pressure ($1/2\,\rho V^2$)
s	wing area
V	airspeed
M	Mach number
α	angle of attack
δ_e	elevator angle, positive down
$\dot{\theta}$	pitch angle
M	pitching moment about y-axis, positive nose up
L	lift, force in plane of symmetry, normal to relative wind, positive up

Symbols and Definitions

Aerodynamic Notation	
C_L	lift coefficient $L/1/2\,\rho V^2 S$
C_m	pitching moment coefficient $M/1/2\,\rho V^2 Sc$
L_α	$(\rho SV/2m)\ C_{L_\alpha}$
L_δ	$(\rho SV/2m)\ C_{L_\delta}$
M_α	$(1/2\,\rho V^2 Sc/I_y)\ C_{m_\alpha}$
M_δ	$(1/2\,\rho V^2 Sc/I_y)\ C_{m_\delta}$
$M_{\dot{\alpha}}$	$(1/2\,\rho V^2 Sc/I_y)\ (\frac{c}{2V})\ C_{m_{\dot{\alpha}}}$

Abstract

This report describes the analog simulation for the longitudinal axis of the General Electric Self-Adaptive Flight Control (GESAC) System, as proposed for use on the X-15 aerospace vehicle.

The gain-changing dynamics of the non-linear loop are considered briefly and the effects of noise on system operation are observed.

A method of optimizing the system simulation by first considering the non-linear loop independently is described in detail.

It is shown that this system is capable of maintaining aircraft stability throughout the X-15 re-entry flight profile and that noise introduced during system operation does not seriously degrade system performance.

ANALOG SIMULATION AND ANALYSIS OF A NON-LINEAR SELF-ADAPTIVE FLIGHT CONTROL SYSTEM

I. Introduction

Purpose

The purpose of this study is to investigate the dynamic behavior of a specific self-adaptive flight control system which incorporates a non-linear frequency sensor in its adaptive loop. By means of analog simulation, a method of optimizing this non-linear loop is presented.

The particular system investigated is the General Electric Self-Adaptive Control (GESAC) system. The system was originally designed for advanced fighter aircraft and has been flight tested in an F-106 type aircraft. It was later modified and proposed for use on the X-15 and the Dyna-Soar lifting re-entry vehicle. This study will consider only the GESAC application to the X-15 type aerospace vehicle.

Defining the Self-Adaptive System

A survey of the literature in the automatic control field reveals a surprising difference of opinion as to what should properly constitute a self-adaptive control system. For the purposes of this study the definition proposed by Rath (Ref 1) will be adopted, i.e., a self-adaptive system is one which forces the response of the controlled element to follow an optimum or model response by sensing internal loop parameters.

The difference between this system and the ordinary adaptive system (such as the air-data system which adapts its response as demanded by the air-data sensing loop) is that in the self-adaptive system, the adjustment is based on measurement of the dynamic response itself rather than on the measurement of some external environmental parameter.

Method and Scope

The GESAC system is analyzed mathematically by use of root locus techniques and by means of an analog simulation. Various flight conditions are selected (Table 1, page 26) which represent a typical re-entry flight path for the X-15. The stability derivatives for these flight conditions are used to find the aircraft transfer functions, and a root locus plot is made for three representative flight conditions (omitting the non-linear frequency-sensor loop).

Background

The increased use of modern high performance aircraft and the genesis of the lifting re-entry vehicle for accomplishing military missions in space have introduced severe aerodynamic stability problems into flight control system design.

In the days of propeller-driven subsonic aircraft with their inherent stability, the pilot was able to control the aircraft throughout its flight envelope by a simple mechanical system of levers and pulleys. As aircraft capability approached Mach 1 the inherent stability decreased and artificial

stability damping became desirable. With the penetration of the sonic barrier, air vehicles have entered the supersonic regime, and stability damping has become mandatory. In addition, the dynamic behavior of the supersonic aircraft demands response times which are not consistent with human reaction times. For these reasons, the latest operational air weapon systems in some instances require completely automatic flight-path control for successful mission accomplishment.

An appreciation of the stability and control problem of high-performance aircraft can be realized by analyzing the assumptions underlying the mathematical solution to the equations of motion of the aircraft. The motion of a rigid body can be completely described by a set of six differential equations. Three equations describe motion of translation of the center of gravity (c.g.) along each of the three axes (u, v, and w), and three equations describe rotation of the aircraft about the c.g. (p, q, r), as indicated in Figure 1.

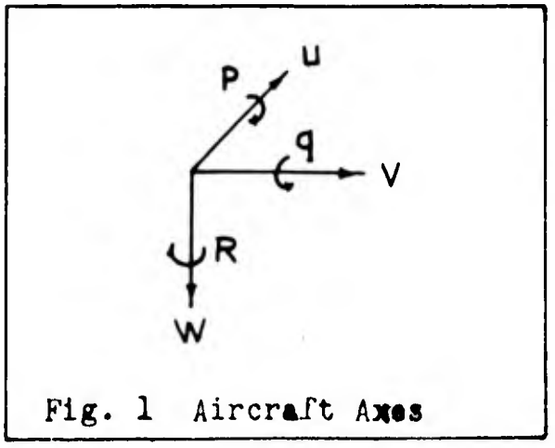

Fig. 1 Aircraft Axes

These equations are normally treated by dividing them into two sets, the first set describing the longitudinal modes (q-pitch rate, u-forward velocity and v-slideslip), and the second set describing the lateral modes (p-roll rate, r-yaw rate and v-slideslip). By assuming that the u-v axes lie in

the plane of symmetry and that p and r undergo only small perturbations, the coupling effects between these two sets of equations can be neglected and the equations more easily handled.

In the transonic and hypersonic regime, the coupling between these equations is increased, partly due to reduced surface effectiveness because of aeroelastic effects and partly due to the large differences in the moments of inertia about the u and v axes. One solution for increasing the surface effectiveness is to increase the control surface. But since increasing the size of the control surface beyond a certain point results in excessive drag, the only alternate solution is to provide some sort of stability augmentation.

Since aircraft characteristics vary with such factors as Mach number, dynamic pressure, and aircraft configuration, the amount of stability augmentation needed also varies with these parameters. The design of previous flight control systems (including some for supersonic aircraft) has relied largely on air-data sensing. That is, the response sensitivity or system gain was scheduled into the system as a function of Mach number or dynamic pressure. This method requires a thorough knowledge of airframe dynamics throughout the flight envelope, which can only be obtained from an extensive flight-test program. This method of air-data control has the disadvantage of being costly, complex and

cumbersome, since each system must be tailored to each individual airframe. In addition, when considering lifting re-entry type vehicles, air-data sensing on the fringes of the atmosphere becomes extremely difficult. It is for these reasons that the concept of a self-adaptive system is considered a major breakthrough in the automatic control field.

Method

The basic equations used are those which describe the longitudinal short-period mode. The phugoid mode is not examined since its period is long enough not to present a control problem. Blakelock gives a detailed explanation of the assumptions made in arriving at these equations. (Ref 2) The major assumptions are that both the effects of speed change and flight path angle on the short-period mode can be neglected. The equations are as follows:

$$\ddot{\theta} = M_q \dot{\theta} + M_{\dot{\alpha}} + M_\alpha \alpha + M_\delta \delta_e \tag{1}$$

$$\dot{\alpha} = \dot{\theta} - L_\alpha \alpha - L_\delta \delta_e \tag{2}$$

From these equations, the transfer function of the aircraft is obtained.

Combining this transfer function with the transfer functions of the other system components yields the characteristic equation of the system. The poles and zeros of the

characteristic equation are plotted and a root locus analysis is made for each flight condition. These results are then compared with the analog computer simulation results, both to check the simulation and to serve as a method of system familiarization. Since the gain-changing loop is non-linear and hence not amenable to description by linear differential equations, it is analyzed solely by means of the analog computer.

Plan of Report

Chapter II contains a description of the system operation with particular emphasis on the operation of the frequency sensor loop. In Chapter III the detailed mechanization of the system as simulated by means of a Reeves Analog Electronic Computer (REAC) is described. Chapter IV presents the analytic investigation in which the root locus method is used and in which a linear fixed-gain system is assumed. Chapter V is devoted to the investigation of the gain-changing dynamics of the frequency sensor loop, and the procedure arrived at for the optimization of this non-linear loop. In Chapter VI the Conclusions and Recommendations for further effort are summarized.

II. System Operation

The Model Concept

The difficulties involved in using normal feedback techniques for solving the flight control problem for high performance aircraft are due not only to the fact that the aircraft dynamics vary rapidly over wide ranges as a function of environment, but that the relationship between the aircraft and its environment cannot be accurately described mathematically. A fixed high-gain linear feedback system used under these conditions results in sluggish response at one end of the spectrum and instability at the other. This dilemma prompted the search for a system which would maintain optimum system gain independent of aircraft characteristics.

Campbell was probably the first to propose the use of a reference model in flight control systems (Ref 7). The idea consists of inserting in the system a filter or model, which represents an ideal transfer function. If the loop gain is kept at a high value, it can be shown very easily that the response of the system can be made independent of aircraft characteristics. Consider the system represented by the block diagram in Figure 2.

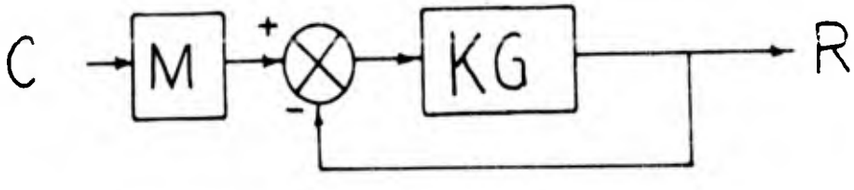

Fig. 2 Block Diagram of System with Model (M) in Prefilter

The transfer function for this system can be expressed as:

$$\frac{R}{C} = M\,\frac{KG}{1+KG} = M\,\frac{G}{\frac{1}{K}+G} \tag{3}$$

As the loop gain K is increased, then

$$\lim_{K\to\infty}\ \frac{R}{C} = M \tag{4}$$

Similarly, if the system were to contain a feedback element as in Figure 3,

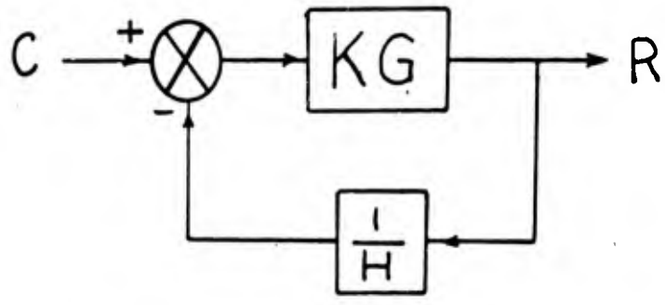

Fig. 3 Inverse Model in Feedback Loop

then $$\frac{R}{C} = \frac{KG}{1+\frac{KG}{H}} = \frac{G}{\frac{1}{K}+\frac{G}{H}} \tag{5}$$

and $$\lim_{K\to\infty}\ \frac{R}{C} = \frac{G}{\frac{G}{H}} = H \tag{6}$$

Thus, the system response is dependent only upon H for conditions of high forward loop gain.

These simple examples illustrate the fact that the model can be placed either at the input as a prefilter, or in the feedback loop as a feedback compensation. A combination of input model and feedback compensation can be used to control independently the response to commands and the response to disturbances. Figure 4 indicates a combined system, where D is a disturbance input.

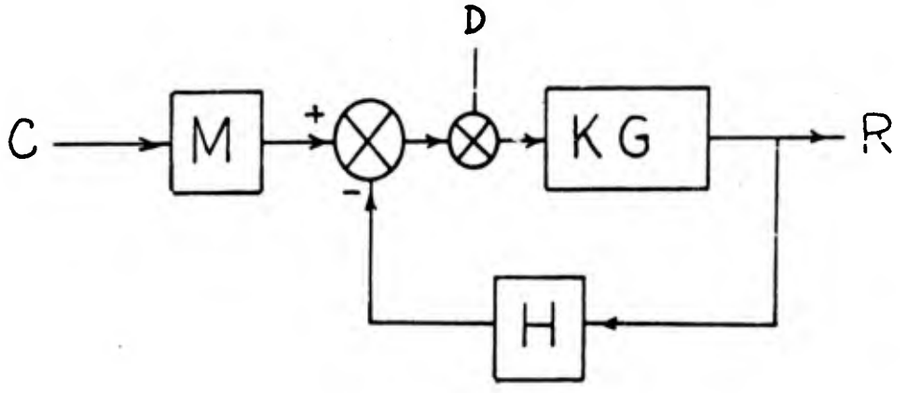

Fig. 4 Combination of Prefilter and Feedback Model with Disturbance

As indicated previously, $\left.\frac{R}{C}\right|_{D=0} = \frac{M}{H}$ for high gain.

In this example $\left.\frac{R}{D}\right|_{C=0} = \frac{KG}{1+KGH}$ (7)

and for high gain $\lim_{K\to\infty} \left.\frac{R}{D}\right|_{C=0} = \frac{1}{H}$ (8)

Therefore, the response to a command input is determined by adjusting M, while the response to the disturbance input can be minimized by increasing the feedback compensation H.

The next question that arises in the study of self-adaptive systems is the feasibility of designing a model possessing the desired characteristics of the air vehicle. The desirable response characteristics for piloted aircraft have been specified in terms of invariant transient response by Chalk and Bull (Ref 3 and 4).

Schuler, et al, have shown how the data representing the desired response can be used to synthesize a model with a second order transfer function, which provides an optimum response for wide ranges of dynamic pressure (Ref 5).

Figure 5 is a block diagram of the GESAC system. The combination of the canceller and direct feedback loops represent the inverse model illustrated in Figure 3. The system designers chose this approach rather than the direct model design in order to provide the system with a better recovery response to disturbances such as a noise or gust input.

Fixed Gain System Operation

If the frequency sensor block in Figure 5 is disregarded, the system would become a linear fixed gain Type 1 servo system. A pitch rate command is passed through the integrator, $\left[\frac{K_1}{P}\right]$, summed with the two feedback voltages (the

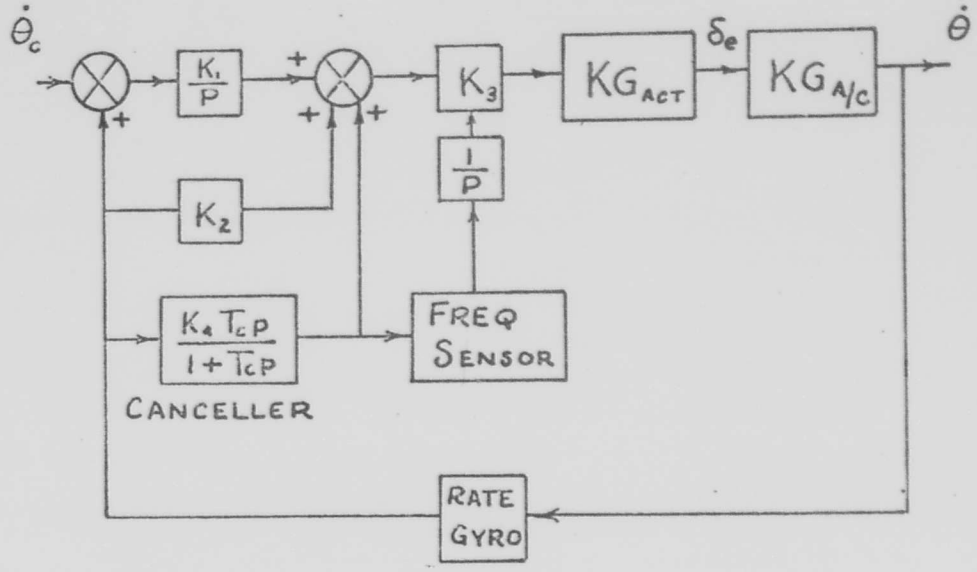

Figure 5 GESAC Block Diagram

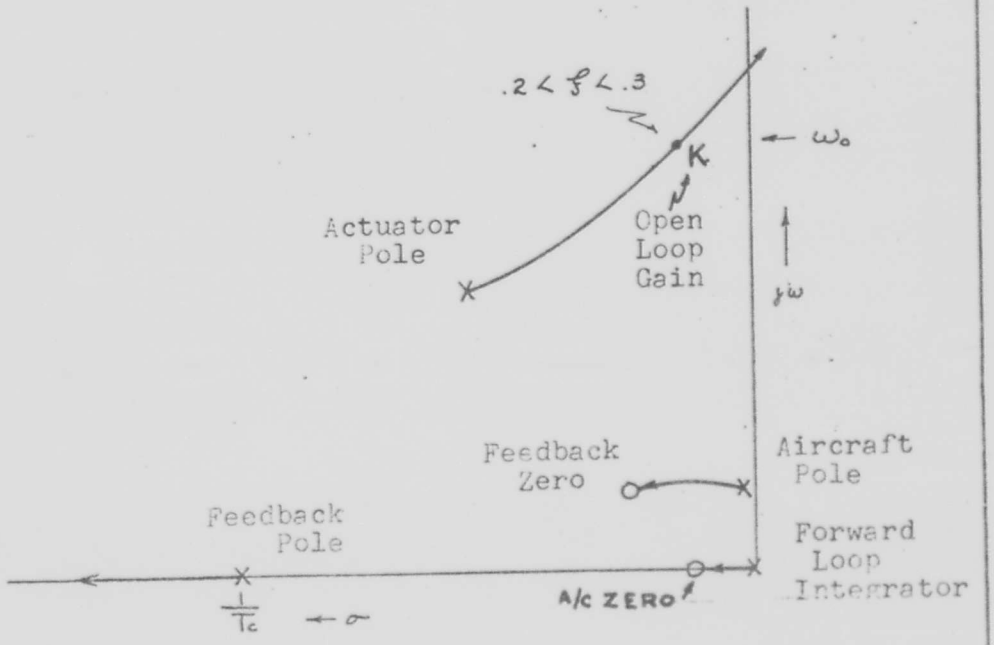

Figure 6 Root Locus Sketch of System

direct $K_2 \dot{\theta}$, and the canceller $\frac{K_4 T_c P}{1 + T_c P} \dot{\theta}$ and multiplied by the fixed gain K_3. This voltage is then applied to the actuator which results in a δ_e signal to the aircraft and in turn a response in pitch rate $\dot{\theta}$.

System operation is best understood by reference to a typical root locus sketch as illustrated in Figure 6. As previously noted, the basic concept depends upon maintaining the open loop gain K sufficiently high so that the closed loop transfer function is essentially determined by the model in the feedback loop. Ideally this response would occur at infinite gain. As the open loop gain K increases, however, the root locus branch originating from the actuator pole (the dominant mode) goes unstable at some finite gain. The objective is to maintain the open loop gain as high as possible, and still keep the system stable.

The operation of the system depends upon providing feedback zeroes which will adequately compensate the aircraft poles. The frequency of the aircraft or control mode varies from 0 to 5 radians per second while the frequency of the dominant mode varies from approximately 28 to 45 radians per second as the open loop gain goes from zero to infinity. As a result of this difference, the frequency at which the dominant mode goes unstable remains relatively fixed as the control mode frequency varies with flight conditions.

In a report of the F-106 flight test evaluation of this system, the authors discuss in some detail the considerations which led to the selection of the frequency of the actuator mode as the criterion for adapting the system response (Ref 6). They also present several methods used in the preliminary design stages for the sensing of this frequency. Since this study is concerned only with the analysis and optimization of the present system, these design factors will not be discussed.

Frequency-Sensor Loop Operation

In the previous section the system was examined as a fixed gain linear feedback system. In this section the operation of the non-linear frequency-sensor loop will be described by reference to Figure 7.

The frequency-sensor loop detects a system variable (frequency) and compares this quantity with the optimum value. When a difference exists, an error signal is sent back to the system which corrects system operation toward optimum again. The input signal goes through a relatively broad band-pass filter $\left[\frac{S^2}{(1+\tau s)^4} \right]$ where τ is chosen so that the peak amplitude of the filter occurs at the reference frequency (ω_o). This filter produces a 12 db/ octave rise and decay around this peak frequency. The purpose of the filter is to isolate the frequency of the mode being detected by the frequency sensor from the lower frequency

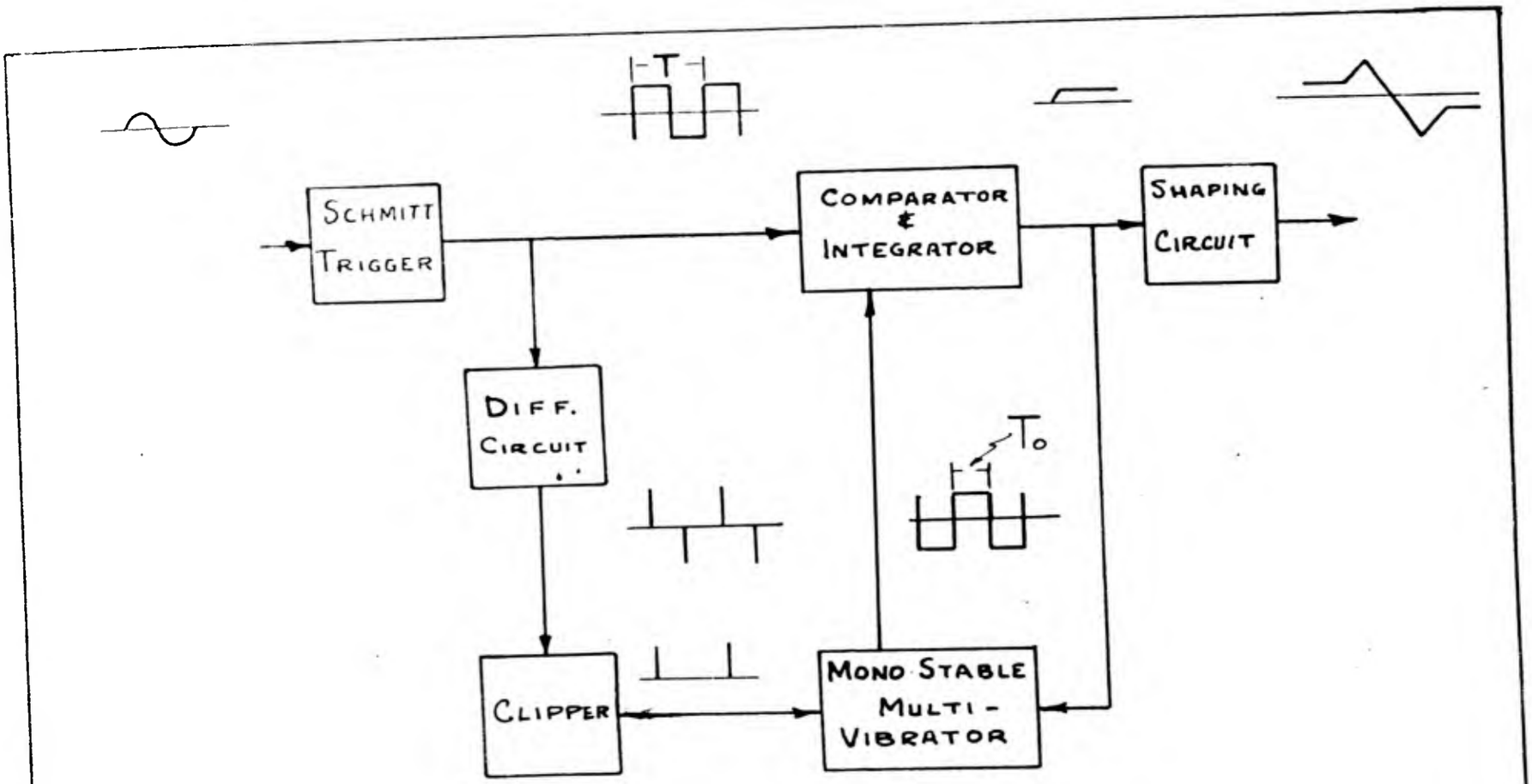

Fig. 7 Functional Block Diagram of Frequency Sensor Loop

aircraft mode or from the higher frequency structural and rate gyro modes. This signal is then passed to a Schmitt trigger circuit which results in an output of constant amplitude peak-to-peak square waves at the frequency of the incoming signal. Since the Schmitt trigger detects only zero crossings of the incoming signal, amplitude variations with frequency within the bandwidth of the input filter will have no effect on system operation. As indicated in Figure 7, this signal is then passed through a differentiator which results in an output of positive and negative spikes representing the positive-going and negative-going voltages of the square wave. The clipper eliminates the negative spike, leaving the positive one to excite a mono-stable multivibrator. The output of the multivibrator is a square wave with a pulse width (T_o) set internally to represent the half period of the desired frequency (ω_o). This pulse occurs at the same frequency and amplitude as the output of the trigger circuit. When the output of the multivibrator is subtracted from the output of the trigger circuit, the difference is integrated and applied through a signal-shaping circuit to a gain-changing servo which changes the system gain so as to make the half period ($\frac{T}{2}$) of the system frequency equal to the half period (T_o) of the multivibrator. When these signals are exactly equal, the system will be operating at its optimum point as seen from the root-locus sketch

(Figure 6). A feedback loop from the integrator to the multivibrator provides for automatic adjustment of T_o in the direction of $\frac{T}{2}$. This serves as a smoothing circuit for the corrective voltage applied to the system. The signal shaper improves the signal-to-noise ratio and limits the voltage applied when there is an extreme difference in the frequency of the system and the frequency of the multivibrator.

In the next chapter the simulation of the overall system, and of the frequency sensor loop in particular, is described in detail.

III. System Simulation

For purposes of description in this chapter the GESAC system will be divided into two main subsystems. The first part described is the outer loop or fixed-gain portion of the system. This includes everything but the frequency-sensor loop which is described separately.

In Figure 8 the system block diagram is shown again for convenience, indicating the location of the frequency sensor by the dashed lines. Figure D-1 (gatefold) in Appendix D illustrates the simulation of the block diagram in Figure 8 with the frequency-sensor loop again enclosed by dashed lines. The transfer functions for the aircraft, actuator, and the canceller in the feedback loop are indicated.

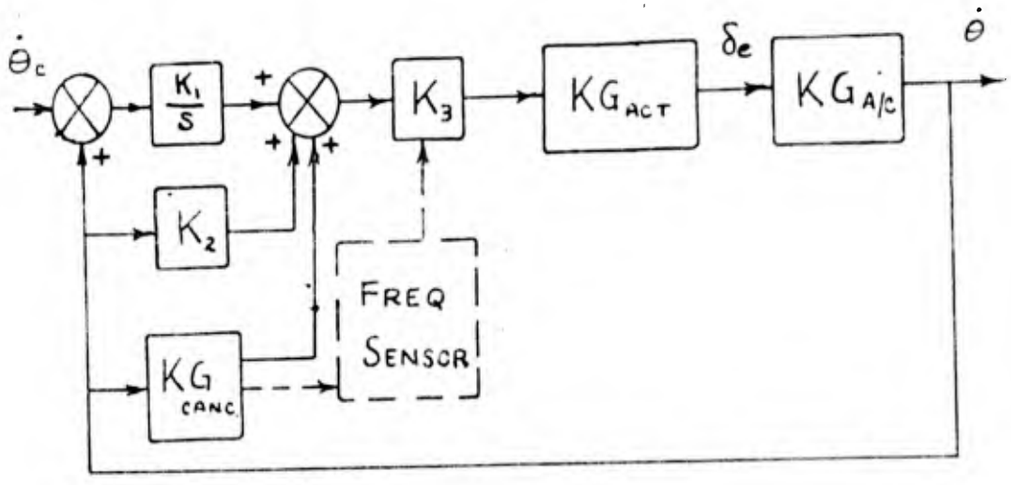

Fig. 8 System Block Diagram

The rate gyro in the feedback loop was neglected in the simulation since its natural undamped frequency is so high (approximately 400cps) that it has negligible effect on the root locus. The potentiometer settings for each flight condition are listed in the appendix.

Frequency Sensor Loop Simulation

As described in Chapter II, the frequency sensor loop consists of a Schmitt trigger circuit, a differentiating and clipping circuit, a mono-stable multivibrator, a comparator, an integrator, and a shaping circuit at the output to the gain-changing servo. The simulation used for the above components is shown in Figure D-1 along with the sine-wave generator which is used for test and calibration.

The frequency sensor loop operates on an error signal which is taken from the canceller circuit in the overall system feedback loop. The frequency of this error signal is then compared with the desired reference frequency (ω_r) generated in the multivibrator circuit, and the difference is represented by a voltage at the output of the frequency sensor loop. After passing through a filter, this voltage is used to drive a servo which varies the system gain to maintain the frequency of the actuator poles equal to the desired frequency of the frequency sensor.

The filtered error signal is first applied to a Schmitt trigger circuit (SU-15 Figure D-1) which senses zero crossings of the input and results in an output of square waves limited to +50v and -25v (see Figure 9). Since the bridge limiters used require an operational amplifier on their output, this square wave appears at the output of SU A-8 limited to +25v and -50v. At this point the signal is split and performs two functions. First it is inverted again by IV A-16 and sent to the comparator and integrator IG A-3 where it will be compared with the square wave out of the multivibrator. The other part of the signal is sent to the differentiating and clipping circuit as indicated in Figure D-1. The positive pulse from the differentiating circuit causes the output of SU A-16 to flip to its negative limit (-25v). This appears as a +25v at the output of SU A-9. The voltage from SU A-9 passes through potentiometer A-89 into IG A-11 resulting in a negative-going ramp from its +25v upper limit. This negative ramp is then fed back to SU A-16 where it is added to the +25v out of SU A-9 and the feedback voltage out of IG A-3. As indicated in Figure 9, whenever the negative-going voltage from IG A-11 balances out the positive voltage at the input to SU A-16, the output of this amplifier will flip position again and the half-period of the multivibrator ends. Potentiometer A-89 controls the

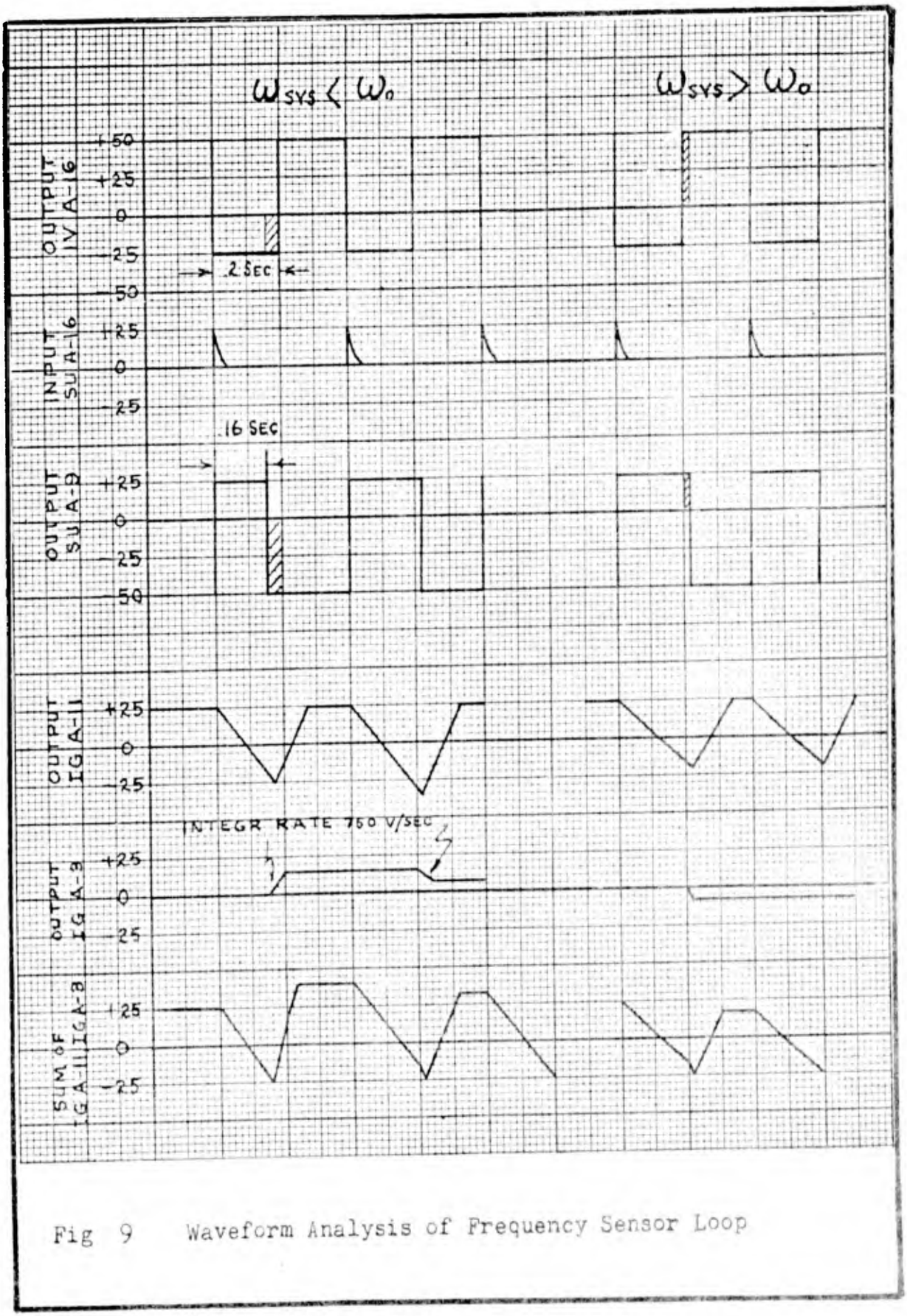

Fig 9 Waveform Analysis of Frequency Sensor Loop

slope of the negative-going ramp out of IG A-11; hence it controls the half-period T_o of the multivibrator.

The limit levels on SU A-16 are adjusted to give a negative limit whose magnitude is twice as great as the positive limit. This is done so that the negative pulse into IG A-11 will return it to its original positive state well within the half-period T_o. Thus, the unequal limits on SU A-16 decrease the recovery time of the monostable multivibrator.

The resulting wave form out of SU A-9 as shown in Figure 9 has a constant peak-to-peak voltage as set by the limiters, an overall period T determined by the frequency of the error signal (system frequency), and a half-period T_o determined by the adjustable integrated voltage out of IG A-11. This square wave out of SU A-9 is then subtracted from the square wave out of the Schmitt trigger and the difference is integrated to obtain a voltage which is proportional to the difference between the reference frequency of the multivibrator and the system frequency. This voltage is then applied through a signal shaper and filter to a servomultiplier which changes the system gain in a manner which makes the system frequency identical with the desired frequency.

The voltage out of IG A-3 is also fed back to SU A-16 where it continually adjusts the half-period of the multivibrator T_o until T_o is equal to $\frac{T}{2}$. The two square waves

are then identical; the input to IG A-3 is zero and the output is proportional to the difference between the system frequency and the desired frequency of the multivibrator.

By means of this feedback voltage, the half-period of the multivibrator is varied about the nominal value set on potentiometer A-89. The effect of this bias voltage is shown in Figure 9. When the system half-period is greater than the multivibrator half-period, the bias voltage is positive and it adds to the positive voltage from SU A-9, thus increasing the time it takes the negative-going ramp from IG A-11 to flip SU A-16 and hence increasing T_o. When the bias voltage is negative ($T_o > \frac{T}{2}$), it subtracts from IG A-11, and T_o is decreased. In this manner, the bias is varied every half-period until the periods of the two square waves are equal. Thus the output of IG A-3 is proportional to the deviation of the input signal from the nominal frequency (ω_o). The dynamic behavior of the frequency sensor is determined in large part by the bias level set on potentiometer A-85. In addition to acting as a smoothing circuit on the error voltage applied to IG A-3, this feedback loop prevents IG A-3 from overloading by keeping the error signal small.

Frequency Sensor Shaping Circuit

As indicated in Figure 10, SU B-1, SU A-13 and IV A-11 followed by pot A-38 all are used to shape the output of

IG A-3 as shown. Pots B-84 and B-85 and the corresponding diodes are used to limit the width of the dead zone caused by the output of SU B-1 cancelling the direct voltage through SU A-13. The output from SU A-13 within this zone is then determined by the pot setting of A-56. The system was calibrated to give a peak output of 40 volts corresponding to a difference between system frequency and ω_o of 5 radians/second. For greater differences of frequency the signal is attenuated. This minimizes the effect of signals due to noise or switching transients that would falsely indicate the need for large corrections in the system.

Sine Wave Generator

The sine wave generator used for calibration and optimisation is shown in Figure D-1 adjacent to the frequency sensor. During calibration the sine wave generator frequency is determined by the setting on pot A-84 (ω_o = 35 radians/second was used as explained in Chapter IV). The voltage out of SU A-7 was then passed to SU A-15 through the frequency sensor filter and pot A-89 adjusted until the output of IG A-3 is zero. This calibration method insures that the half-period of the mono-stable multivibrator coincides with the desired ω_o . This sine wave generator was also used to optimize the frequency sensor loop as described in Chapter IV.

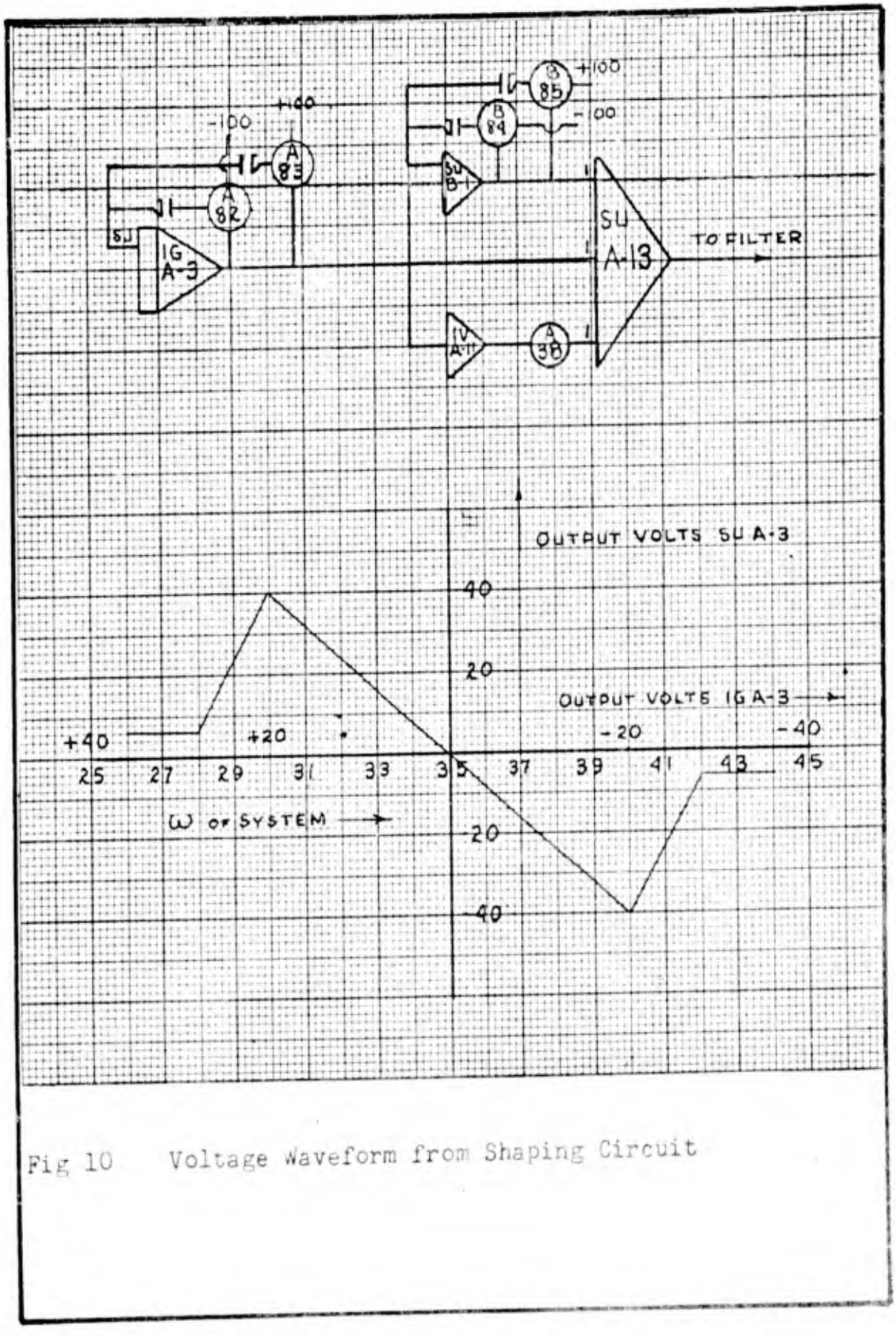

Fig 10 Voltage Waveform from Shaping Circuit

IV. Analytic Investigation

Root Locus Analysis

Assuming the system operates as a linear, fixed-gain (K_3) system, it is possible to analyze the system operation by means of root locus techniques. In order to use the root locus method, the fundamental equations describing system properties must be written in transfer function form for each component.

From the equations of motion of the aircraft

$$\ddot{\theta} = M_q \dot{\theta} + M_{\dot{\alpha}} \dot{\alpha} + M_\alpha \alpha + M_\delta \delta_e$$

$$\dot{\alpha} = \dot{\theta} - L_\alpha \alpha - L_\delta \delta_e$$

the following transfer functions in Laplace notation result.

$$\frac{\dot{\theta}(s)}{\delta_e(s)} = \frac{s(M_\delta - L_\delta M_{\dot{\alpha}}) + M_\delta L_\alpha - M_\alpha L_\delta}{s^2 + s(L_\alpha - M_q - M_{\dot{\alpha}}) + (-M_\alpha - M_q L_\alpha)}$$

$$\frac{\alpha(s)}{\delta_e(s)} \qquad \frac{s(-L_\delta) + M_\delta + M_q L_\alpha}{s^2 + s(L_\alpha - M_q - M_{\dot{\alpha}}) + (-M_\alpha - M_q L_\alpha)}$$

From the above equation for $\frac{\dot{\theta}(s)}{\delta_e(s)}$ the natural undamped frequency and damping ratio may be expressed as:

$$\omega_n = (-M_\alpha - M_q L_\alpha)^{\frac{1}{2}}$$

$$\zeta = \frac{L_\alpha - M_q - M_{\dot{\alpha}}}{2\omega_n}$$

The flight conditions (Table I) selected for which the X-15 stability derivatives were evaluated represent a typical re-entry mission profile. A sample calculation for the

t = 90 second case is shown in Appendix A. Table A-1 presents the numerical data used to evaluate the stability derivatives for each flight condition. Using these data and the equations for ω_n and ζ the results shown in Table II were obtained.

Table I

X-15 Flight Conditions

α = angle of attack

$q = \frac{1}{2} \rho V^2$

t	h 1000ft	M Mach #	q (psf)	α (DEG)
0	226	5.6	22.1	0
20	211	5.3	26	0
40	147	5.5	92.1	0.4
60	102	5.9	676	2.6
74	80	5.4	1042	5.0
90	77	4.8	860	1.1

Table II

Variation of Aircraft Parameters with Flight Conditions

ω_n = undamped natural freq.
ζ = damping ratio

t	ω_n	ζ
0	0.396	0.00391
20	0.563	0.00542
40	1.229	0.0101
60	3.330	0.0289
74	5.140	0.0475
90	4.130	0.0551

In order to outline the method used in the root locus analysis, the values for t = 90 sec will be shown in this illustration. The remaining flight conditions for which the root locus plots are shown, were evaluated in a similar manner.

Using values at t = 90 sec the aircraft equations become:

$$\ddot{\theta} = -0.1322\,\dot{\theta} - 0.0463\,\dot{\alpha} - 1.71\,\alpha - 12.2\,\delta_e$$

and

$$\dot{\alpha} = \dot{\theta} - 0.2767\,\alpha - 0.0372\,\delta_e$$

For this case the aircraft transfer function of interest becomes:

$$KG_{A/C} = -\frac{12.2\,s + 2.75}{s\,(s^2 + 0.455\,s + 17.14)}$$

The transfer function for the X-15 actuator as described in Reference 5 is:

$$KG_{ACT} = \frac{1000}{s^2 + 31.6\,s + 1000}$$

The system block diagram (Figure 8) is simplified for analysis and put in the form of Figure 11. The details of this block diagram manipulation are shown in Appendix A.

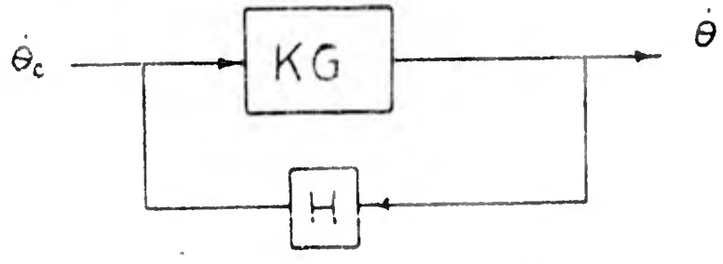

Fig. 11 Simplified Form of System Block Diagram

The transfer function of the system is now of the form $\frac{KG}{1+KGH}$. The characteristic equation $1+KGH$ is then plotted in the complex frequency plane and by means of the root locus technique the system static loop sensitivity K' at which the system becomes unstable is calculated. The corresponding value of the variable gain K_3 can then be computed as indicated in Appendix A.

Figure 12 shows a composite root locus of the flight conditions for t = 0 sec, t = 74 sec, and t = 90 sec. The t = 0 sec and t = 74 sec cases are the extremes within which the aircraft parameters vary and the t = 90 sec case is indicated since it was the one used for the optimization on the analog computer.

Selection of an Optimum ω_o

Before attempting to optimize the frequency sensor loop, it is necessary to select an optimum reference frequency. This selection is made by analyzing the root locus plots in Figure 12. The frequency of the dominant mode (due to the actuator) is limited on the high side by system instability and on the low side by both too high a damping ratio and a too low an undamped natural frequency. The recommended damping ratio for desirable system response is $0.2 < \zeta < 0.3$ (Ref 5). For the t = 90 sec case the $\zeta = 0.2$ point occurs at $\omega = 35.5$ on the root locus and the $\zeta = 0.3$ at $\omega = 32$. These points define the limits on the choice of ω_o.

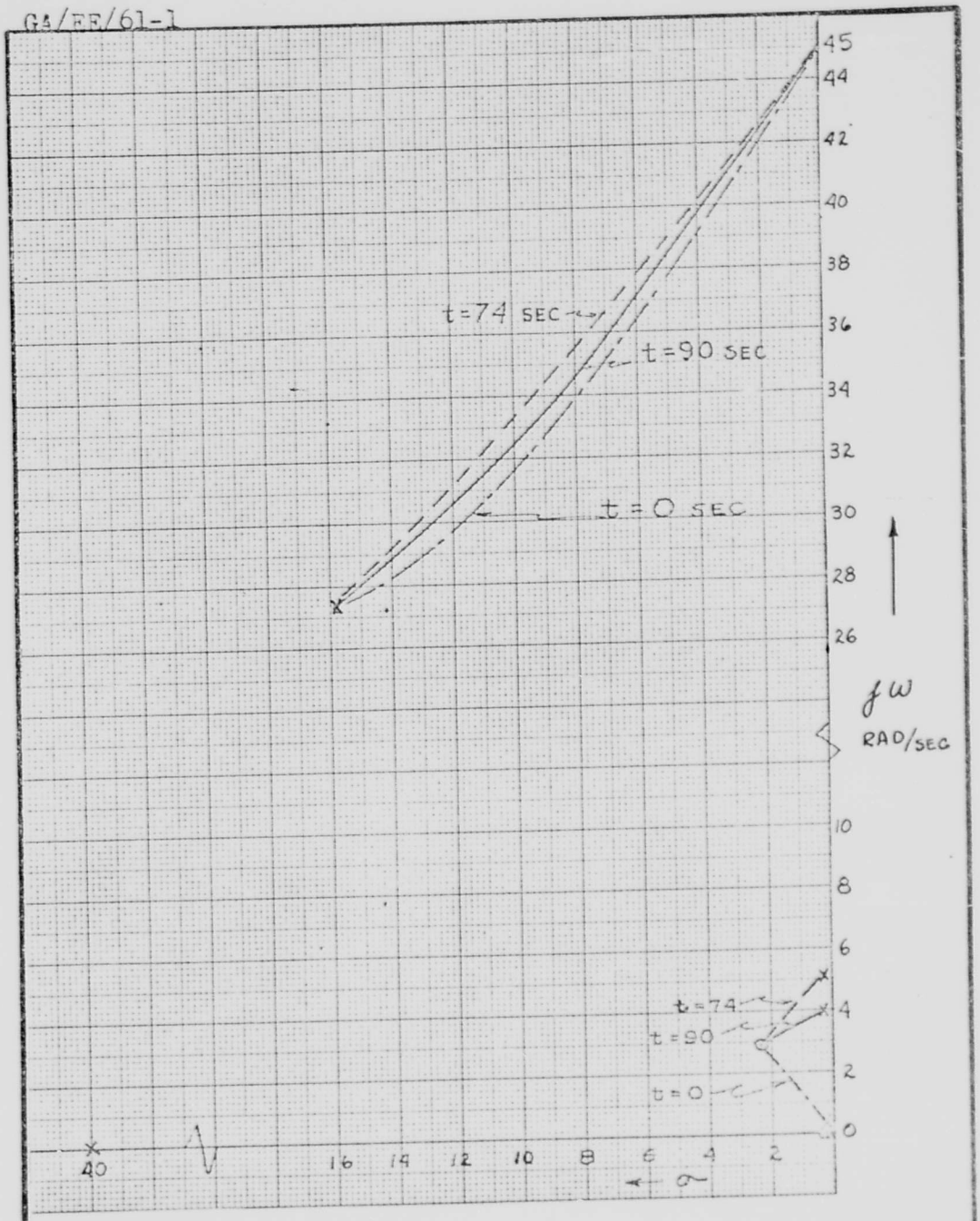

Fig. 12 Root Locus Plots for Three Representative Flight Conditions

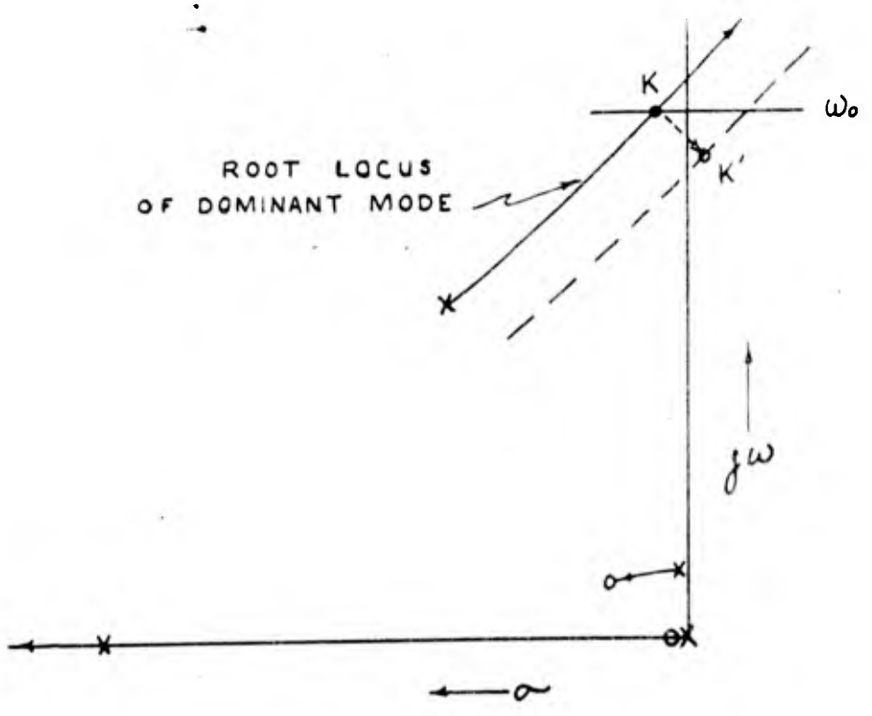

Fig. 13 Effect of Locus Variation on High ω_o Setting

One of the factors to be considered before selecting an ω_o is the maximum expected excursion of the dominant mode closed-loop poles as a function of static loop sensitivity. Another closely related consideration in the actual system is that the locus of the dominant mode may change due to variation in actuator or rate gyro time constants. As shown in Figure 13, if ω_o was set for too high a gain near the imaginary axis and the root locus were to "jump" to the right, the closed loop pole would be below ω_o and

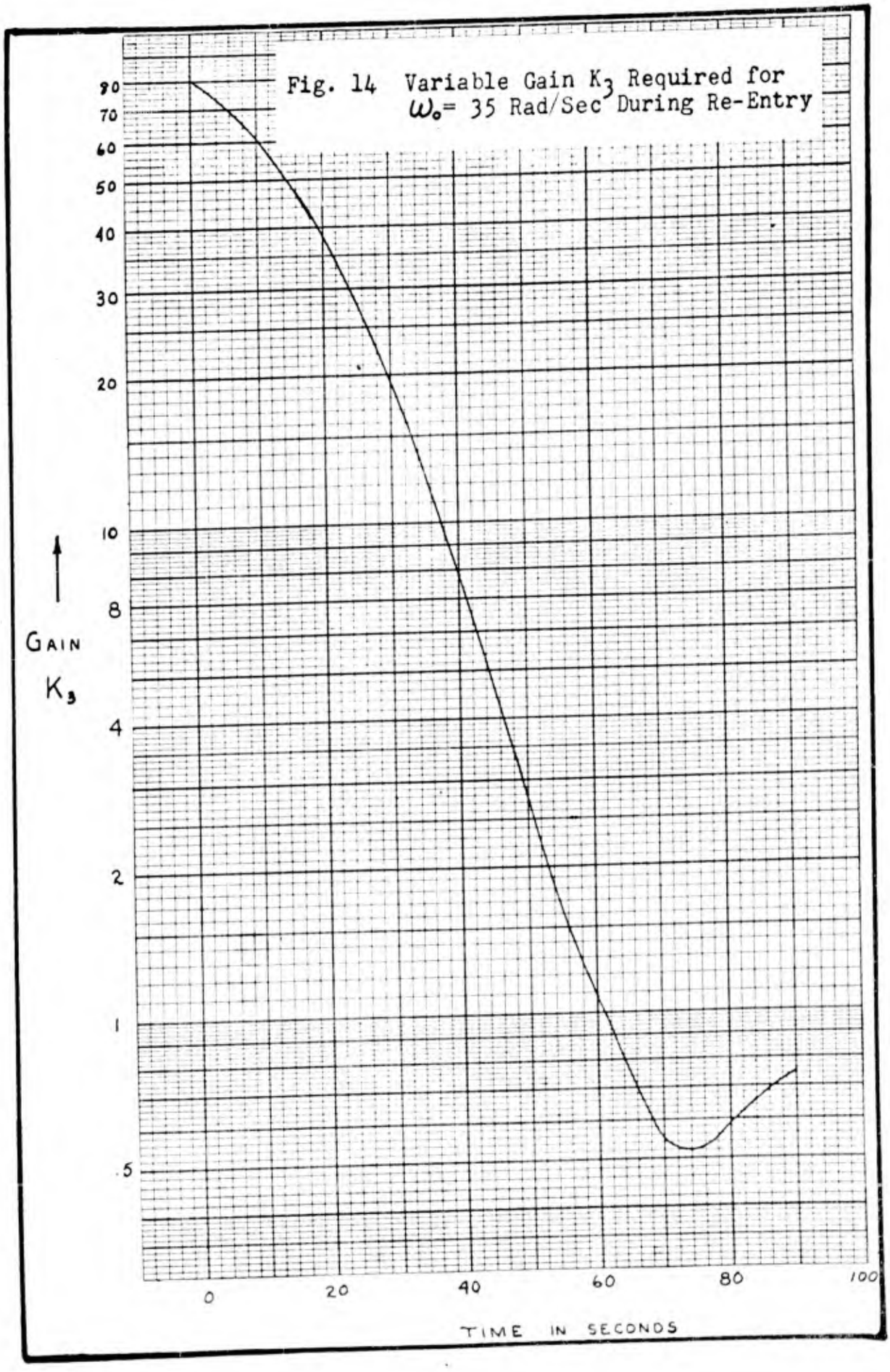

Fig. 14 Variable Gain K_3 Required for ω_o= 35 Rad/Sec During Re-Entry

the frequency sensor would sense the system frequency as being too low and try to increase the gain, thus making the system even more unstable. This is obviously an undesirable situation in an automatic flight control system. As a result of the above considerations, an optimum reference frequency ω_o = 35 rad/sec was selected.

From the root locus plots, the variable gain K_3 required to maintain the dominant mode at ω_o = 35 rad/sec was calculated. The gain K_3 required vs time for the re-entry path chosen is shown in Figure 14. Figure 15 illustrates the rate of change of K_3 with ω for the t = 0 and t = 90 sec case, and Figure 16 presents a plot of the rate of change of $\omega_{n\ A/c}$ with time during the re-entry phase. The data from which these curves were plotted were obtained from the root locus plots for the various flight conditions. The data presented here will be used in the next chapter in conjunction with the results from the analog simulation.

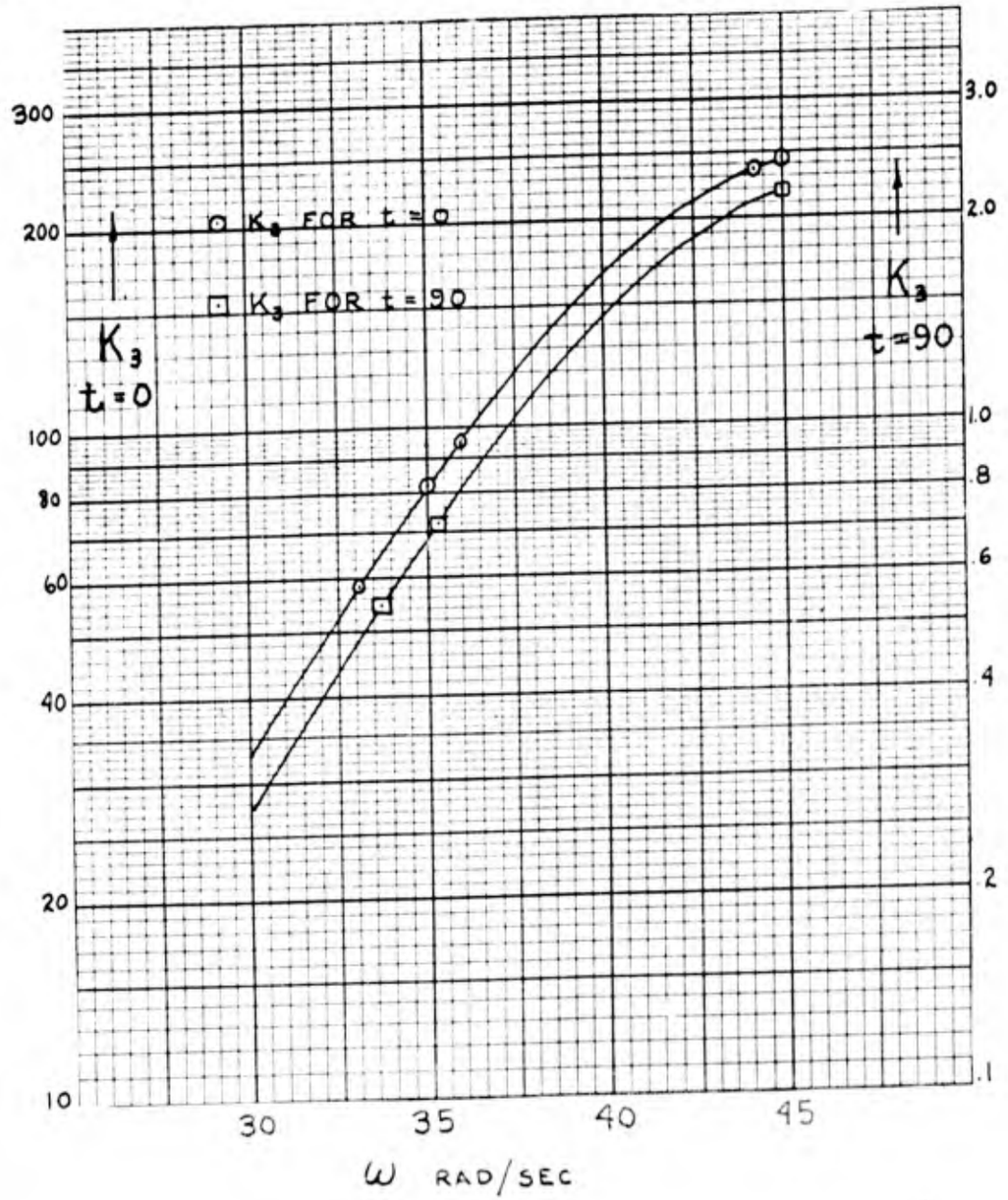

Fig. 15 Variation of Gain K_3 with Frequency for the Two Extreme Flight Conditions

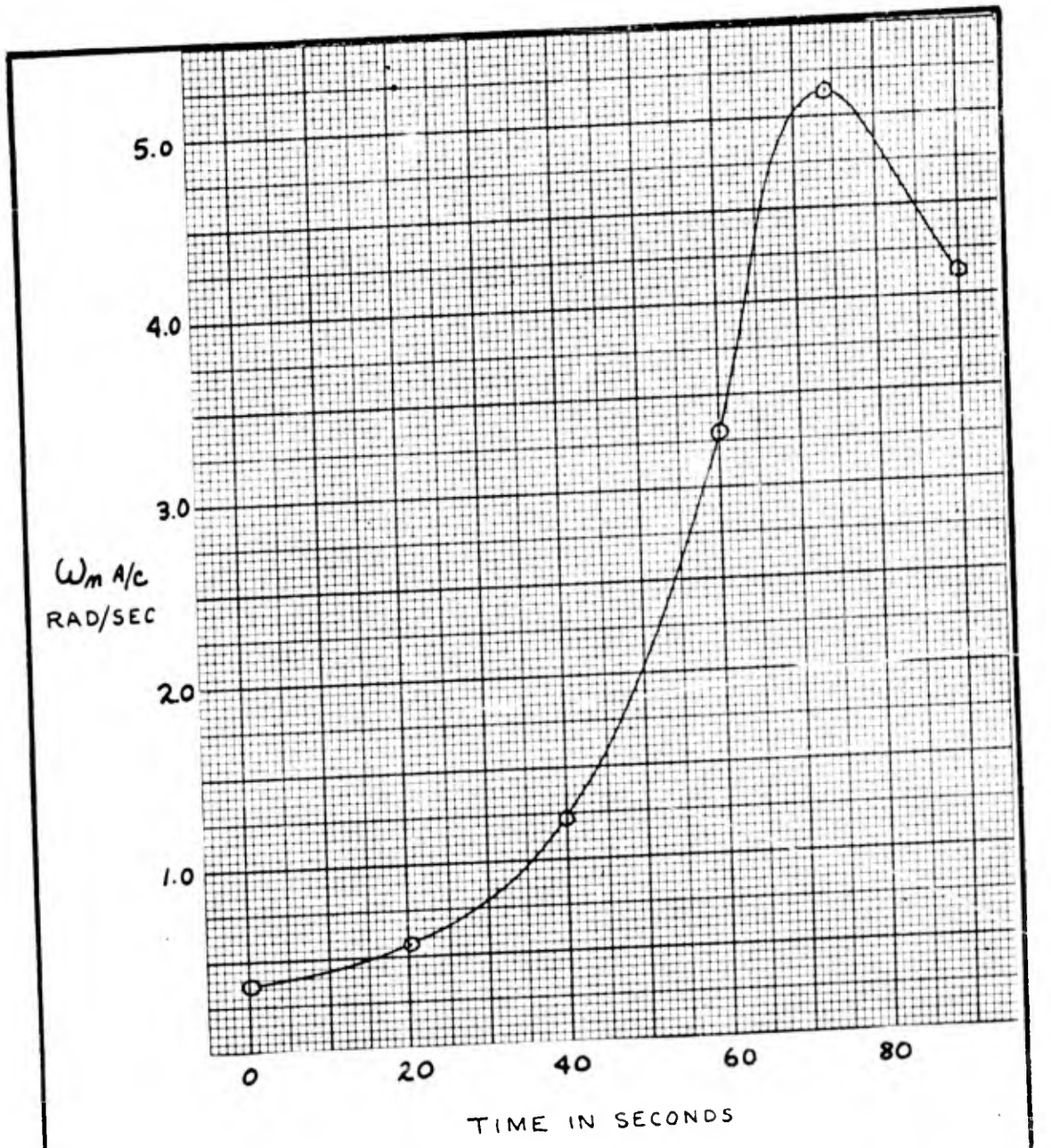

Fig. 16 Variation of ω_{m} A/C with Time During Re-entry

V. REAC Optimization of System and Investigation of Gain Changing Dynamics

Ideally system optimization should simulate the system environment as closely as possible. In this case that would require changing the parameters of the controlled element with time in a manner similar to the actual X-15 re-entry. Since the analog computer did not permit this flexibility, it was necessary to take a given flight condition and check the response of the system to a step input with those particular parameters. The flight condition chosen for the original optimization was at t = 90 seconds. As indicated in Table I page 26, this flight condition occurs at h = 77,000 ft, M = 4.8, and q = 860 lbs/sq ft which is representative for all flight conditions below this altitude.

Simulation Check-Out and Calibration of the Outer Loop

Before system optimization was attempted, the outer loop part of the system (everything except the frequency sensor loop) was first checked to insure that it was a valid simulation of the original system. The open loop aircraft transfer function was checked by measuring the response of the uncontrolled aircraft to a step input. Examples of this response are shown in Appendix C. The undamped natural frequency and damping ratio obtained from this response on the computer was

then compared with the value obtained from the mathematical transfer function.

After the uncontrolled aircraft response was checked, the closed loop system was then connected, omitting the frequency sensor loop. The system gain (K_3) was then increased until the response from the computer indicated instability. The gain (K_3) and frequency at which the system became unstable was then compared with the values obtained analytically from the root locus plots. An additional check on the root locus solutions was made by digital computer runs as mentioned in the Preface. These values are listed in Table III below.

Table III

Root Locus vs Computer Values of Gain K_3 at System Instability

	Values of K_3 at Instability		
t	Root Locus	REAC Results	Digital Results
40	22.7	24.9	23.8
60	3.25	3.20	—
74	1.62	1.60	1.57
90	2.15	2.08	2.24

Error Criterion

The error criterion chosen for this optimization procedure is the integral of the time multiplied by the absolute error (ITAE). This error is defined as: $|\mathcal{E}| = |\dot{\theta}_c - \dot{\theta}|$. This particular error criterion was chosen since it best reveals that error contribution due to both rise time and settling time (Ref 8). These two transient response parameters are of particular importance in optimizing the flight control system response. This circuit for mechanizing error criteria (ITAE circuit) is illustrated in Appendix D, Figure D-1.

Independent Optimization of Frequency Sensor Loop

The optimization of the frequency sensor loop was first attempted while it was operating with the complete system. Due to unpredictable interactions between the frequency sensor loop and the system, it was decided to disconnect the frequency sensor loop for preliminary optimization and work with it independently. This was accomplished by passing the output voltage (proportional to the difference in frequency of the input signal and the reference frequency) into a servo driven sine-wave generator which provided the input signal to the frequency sensor loop. This is shown on Figure D-1 as the calibration hook-up when function switch B-2A is in the up position. The sine wave generator now takes the place of the aircraft, actuator and inverse model by providing the

signal to the frequency sensor and at the same time receiving the error signal from the output of the frequency sensor. This arrangement makes it possible to optimize the non-linear gain-changing loop for best transient response without the complicating interaction of the rest of the system. This procedure of treating the inner loop separately is similar to methods used in the synthesis of linear systems with multiple loops. Here the inner loop gain is first adjusted, followed by gain adjustment for successive loops which sets the poles for each loop to the desired values for optimum transient response.

When this independent optimization has been completed the frequency sensor is reconnected to the system and the potentiometers are adjusted to compensate for the changed response due to the aircraft and actuator in the closed loop. Appendix B contains the itemized procedure and sample calculations for optimizing the frequency sensor loop. The procedure will be outlined in general terms here.

It can be seen from reference to the frequency sensor simulation in Figure D-1 that the potentiometers influencing the gain changing dynamics are: pot A-85, which determines the bias feedback; pot A-89 which determines ω_c, the center frequency; pot A-38 which determines the slope of the shaper output; and pot B-87, the gain into IG A-5. The setting for pot A-89 is determined by the original calibration for

ω_o as described earlier. Pot A-38 was originally set to give a slope of 2:1 within the dead zone limits in order that the maximum error signal occurred at ± 5 radians/second from the center frequency. The approximate value of pot A-85 was calculated as indicated in Appendix B. With reference to Figure 9 page 20, it can be seen that the voltage fedback through pot A-85 is added algebraically to the voltage out of IG-11 to determine the point in time at which the output of SU A-16 flips, thus ending the half-period of the multivibrator. If this voltage is too large, it is evident (for the $\omega < \omega_o$ case) that the second half-period will be much longer than the first thus overcorrecting T_o, and in the limiting case tending to make the system unstable. Thus the setting of this potentiometer has an important effect on the gain changing dynamics of this loop. This is discussed in detail in Appendix B.

The above procedures accounted for all of the attenuation settings except for B-87, which can be represented as the loop gain. In order to optimize this setting a series of runs were made with the sine wave generator set at frequencies of ± 5 radians/second from the center frequency ($\omega_o = 35$) corresponding to maximum error signal from the shaping circuit. Pot B-87 was set at increasing increments of 0.05 for each run and the output of the ITAE circuit was

measured at the end of 10 seconds for each setting. Note that for this procedure, the error signal for the ITAE circuit is provided from the output of IG A-5. The pot setting resulting in minimum ITAE was taken as the optimum. The results are shown in Figure 17. This plot indicates that for a sine wave generator frequency (ω swg) of 40 radians/second, the ITAE minimum occurred at a slightly lower value than for an ω swg of 30 radians/second. This is another indication of the fact that the system corrects itself faster when the system frequency starts to go too high toward the unstable right-half of the complex frequency plane. There are two reasons for this behavior. The first, most obvious one is that as the system frequency goes higher this also increases the pulse repetition rate of the multivibrator. The corrective loop therefore senses more samples per unit time and is able to compensate by adjusting gain more rapidly. The second reason is indicated by reference to Figure 9 page 20. For the case where $\omega > \omega_o$, the voltage out of IG A-11 is added to the voltage fedback from IG A-3 during the first time period that an error is detected. The corrective process in this case starts a cycle sooner, and on succeeding samples the bias feedback from IG A-3 continues to be applied simultaneously with the error detection. This action enhances the system response as a whole, since it is when the system frequency tends toward instability that it

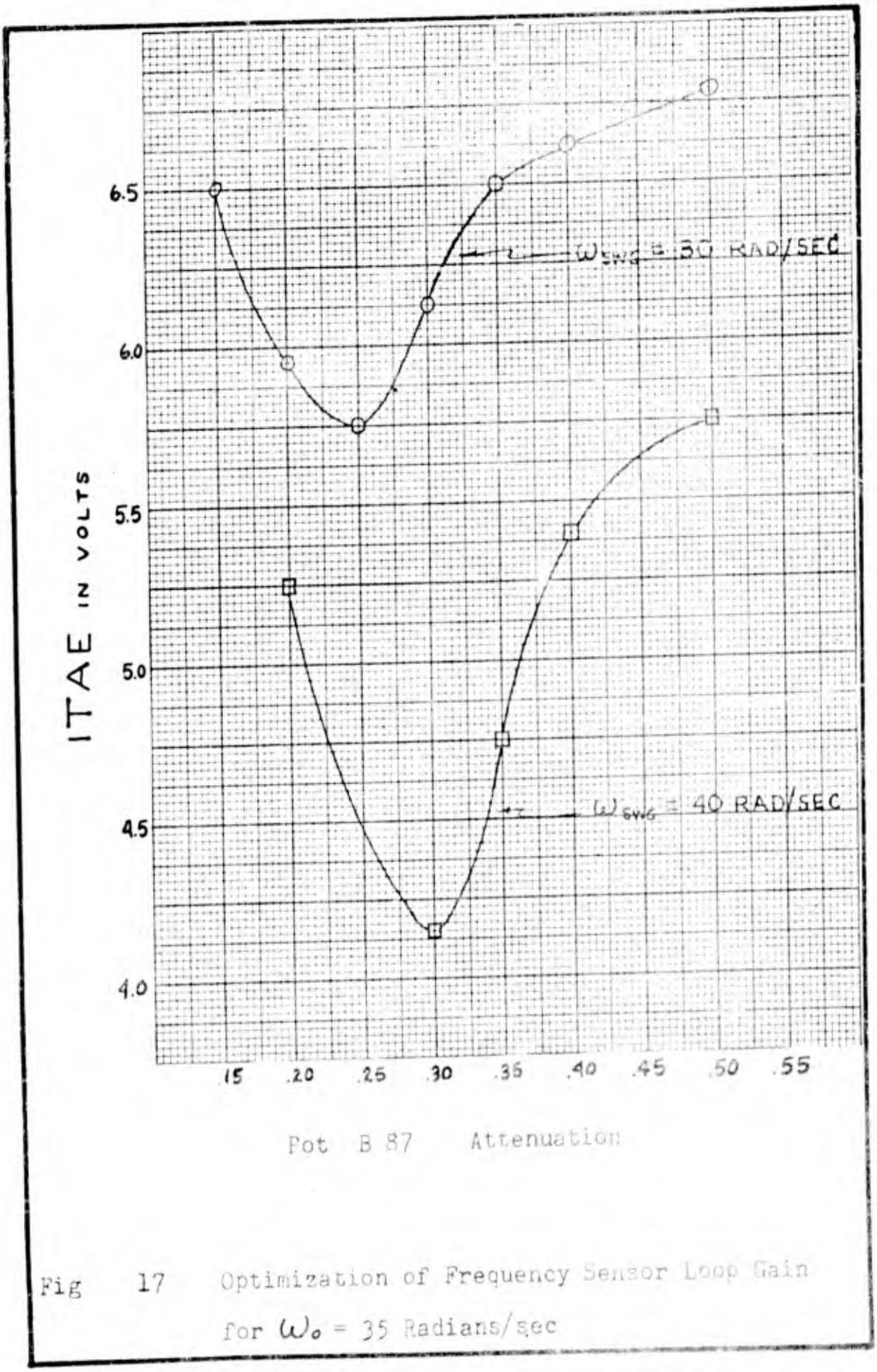

Fig 17 Optimization of Frequency Sensor Loop Gain for ω_o = 35 Radians/sec

becomes advantageous to correct back as quickly as possible. With the attenuation due to pot B-87 optimized, pot B-85 in the feedback loop from IG A-3 can now be adjusted for optimum transient response of the system, either by setting for minimum ITAE as described above, or by reference to the output of IG A-3.

Optimization of Complete System

After the non-linear loop was optimized as described above, it was then connected into the complete system (FSW B-2A Figure D-1 in Down position). The setting for pot B-86 was calculated for K_3 desired when $\omega_{sys} = \omega_o = 35$ radians/second as indicated in Appendix B.

The response of the system to a step input $\dot{\theta}_c$ of 3 degrees/second (6 volts) was then recorded as indicated in Figure 18a. In this figure, the step input is superimposed on the response for comparison purposes. The excess lag indicated here in the system response was originally thought to be due to interaction between the frequency sensor and the remainder of the system. However with the frequency sensor disconnected and with K_3 fixed at a high gain, the best response obtainable from the system is indicated in Figure 18b. In order to compensate for the lag in the $\dot{\theta}$ response a lead-type prefilter $\frac{T_1 s + 1}{T_2 s + 1}$ was added as shown in Figure D-1. As explained in Chapter II, the response

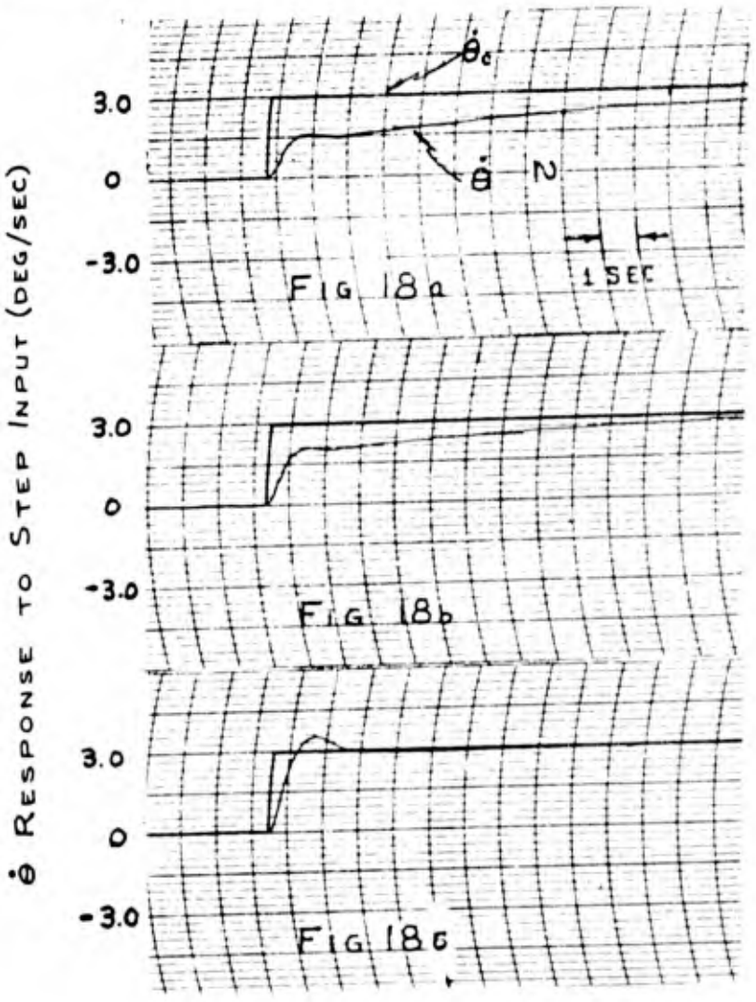

Fig 18a Original Response of System

Fig 18b Response of Fixed, High Gain System

Fig 18c Response of Fixed, High Gain System with Prefilter

to a command input is readily optimized by adjusting the prefilter. The time constants T_1 = 1.5 sec and T_2 = 1 sec were chosen for optimum transient response as shown in Figure 18c.

The frequency-sensor loop was then reconnected to the system and pot B-87 was readjusted for minimum ITAE. The transient response for a step input remained as shown in Figure 18c.

Figure 19 illustrates the voltage waveforms from the frequency sensor during typical operation. For the results shown in this figure, the sine wave generator was offset first to 40 radians/sec and then to 37 radians/sec before the system was turned on. Immediately the corrective voltage out of IG A-3 started to correct the system back to ω_o = 35 radians/sec. The gain-changing loop took approximately 3 seconds to correct for both a $\Delta\omega$ of 5 radians/sec and a $\Delta\omega$ of 3 radians/sec, which is another indication that at higher frequencies, the transient response per unit rate of gain change is improved. The servo multipliers used in this problem had an acceleration limit of 900 volts/sec and a velocity limit of 140 volts/sec, therefore the effect of this equipment on the transient response of the system was negligible.

Figure 20 illustrates the typical operation of the complete system including the frequency-sensor loop, in

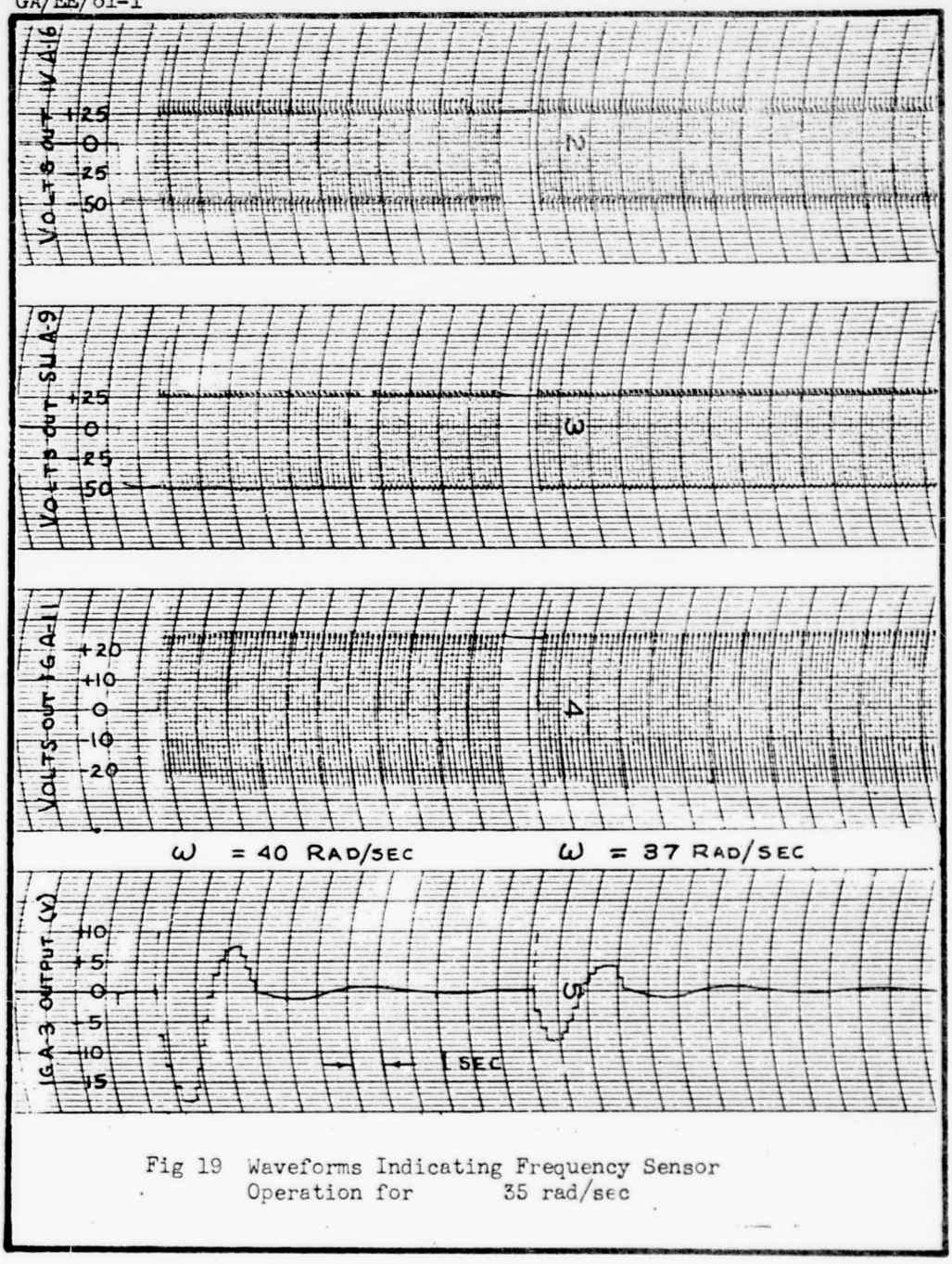

Fig 19 Waveforms Indicating Frequency Sensor Operation for 35 rad/sec

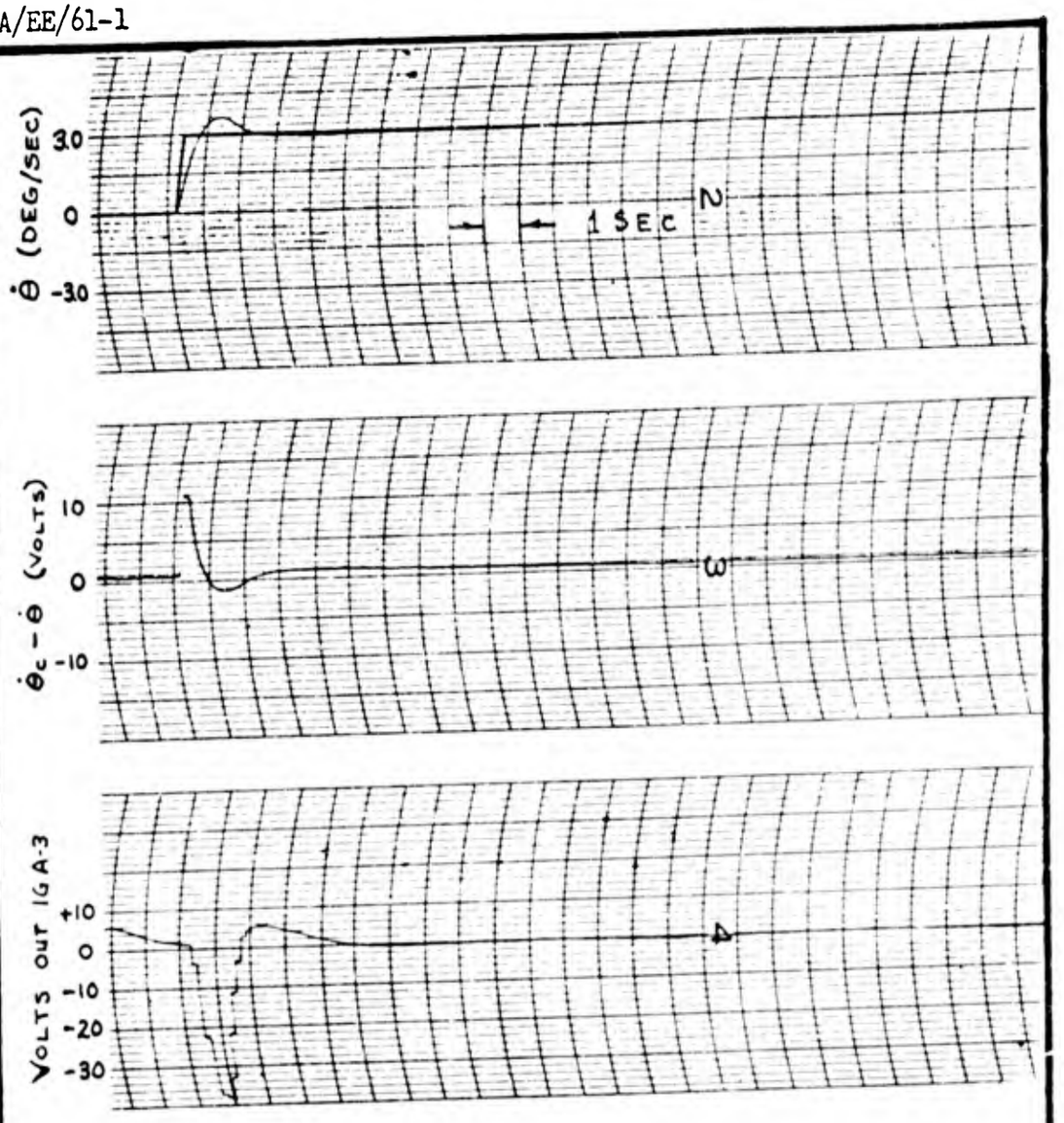

Fig 20 Typical Operation of Complete System on Simulator

response to a $\dot{\theta}$ step input. Other examples of system operation are contained in Appendix C.

Gain Changing Dynamics

The gain changing dynamics of the frequency-sensor loop are examined for only the t = 0 and the t = 90 sec cases, since these two cases represent the two extreme requirements for gain changing capability.

For the t = 90 sec flight condition it is shown from the computer trace in Figure 19 that the system is capable of correcting from a system frequency of ω = 40 to ω = 35 radians/sec in approximately 3 sec. From Figure 15, this would represent a rate of change of K_3 with time $\left(\frac{\Delta K_3}{\Delta t}\right)$ of approximately 0.25 units/sec. This is compared with the slope of the curve in Figure 14 which gives a maximum $\frac{\Delta K_3}{\Delta t}$ in the t = 90 sec region of only 0.04 units/sec, indication that the system has a more than adequate gain-changing capability for stable operation in this flight regime.

For the t = 0 sec flight condition, using the same type of calculation, the system is capable of changing gain at a rate of units/sec (from Figure 15 and Figure 19) and the change of K_3 required (Figure 14) is only 2 units/sec. Based on the data obtained it would appear that the system has adequate gain-changing capability throughout the re-entry flight profile.

Effects of Noise on System Operation

Figures 21 and 22 indicate analog results of the deterioration of system operation when subjected to unfiltered noise inputs at δ_e and α respectively. It is noted that the noise inserted in α causes the system to go slightly unstable. However the frequency sensor is capable of recovering system stability immediately.

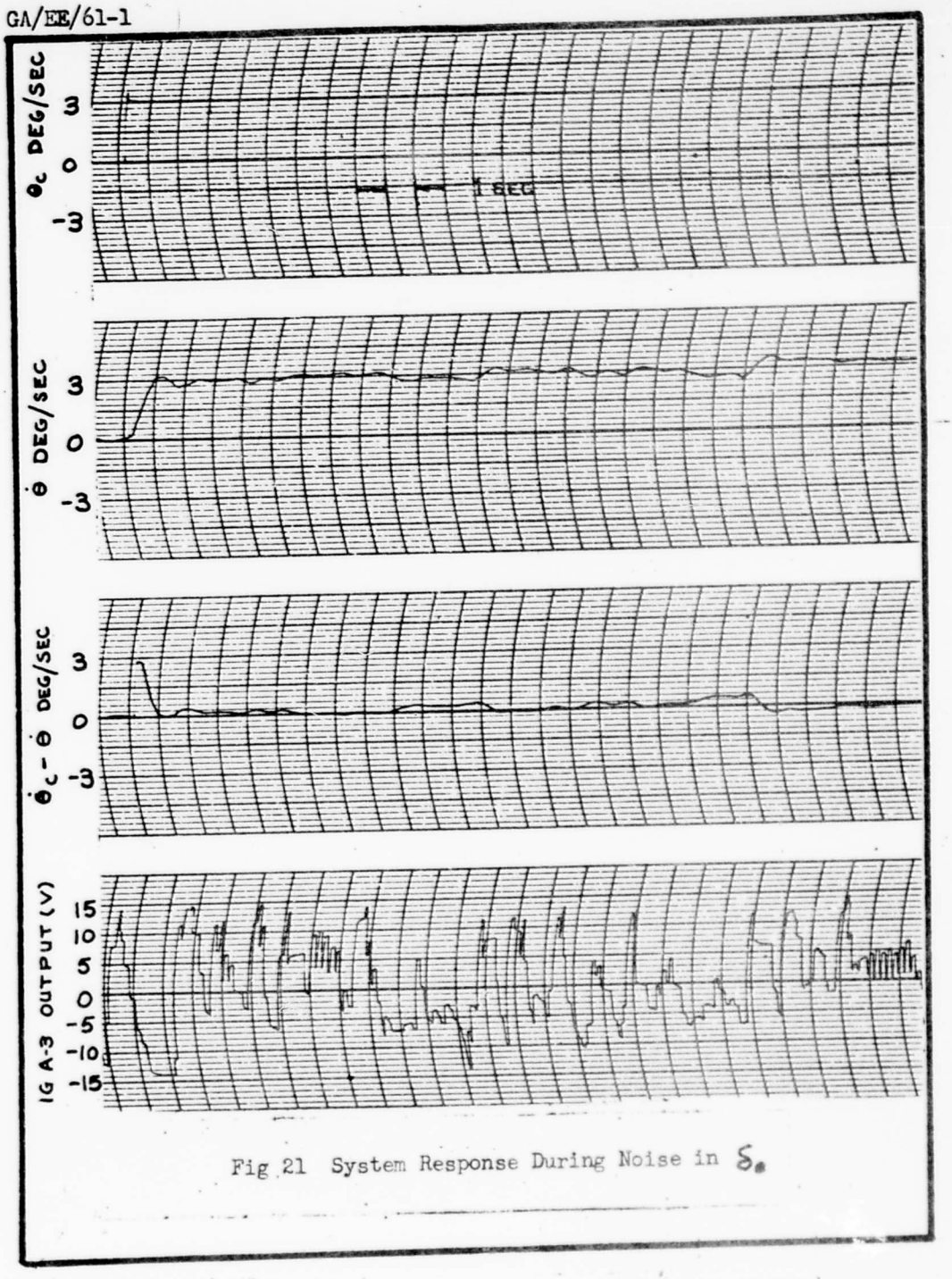

Fig 21 System Response During Noise in δ_e

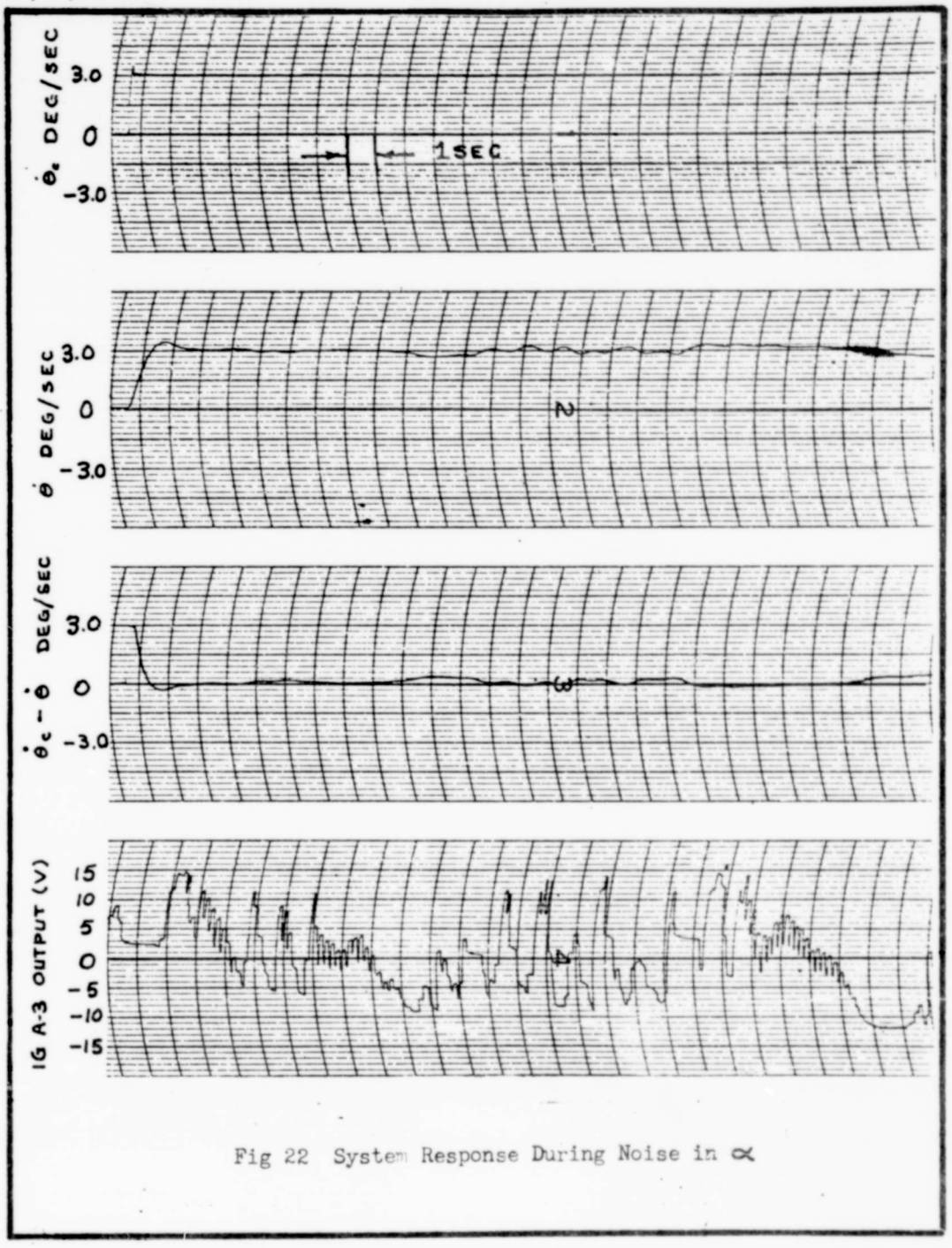

Fig 22 System Response During Noise in α

VI. Conclusions and Recommendations

Conclusions

Several conclusions can be formed as a result of this investigation. They are as follows:

1. The GESAC system as simulated in this study operates satisfactorily in maintaining system stability throughout the normal X-15 re-entry flight profile.

2. Based on the simulation described in the foregoing, the system transient response can be improved by addition of a pre-filter which inserts lead compensation into the system.

3. The system responds well in the presence of noise levels up to 15 volts introduced into both δ_e and α .

4. Where variation of component time constants with environment (temperature, etc.) cause extreme variations in the location of the root locus, it is theoretically possible for the system to go into unstable divergent oscillation.

Recommendations for Future Efforts

1. It is recommended that representative flight conditions on the extreme boundaries of the X-15 re-entry envelope be simulated with this system in order to more adequately define system limitations.

2. An important area for further effort would be an investigation of the effects on the system transient response of variations in component (actuator, rate gyro, etc) time constants due to environmental changes.

Bibliography

1. Rath, Raymond R. Investigation of a Technique for Improving Aircraft Response Using a Complementary Optimum Response "Model". WADC TN56-475, Sep 1956.

2. Blakelock, John H. Automatic Flight Control, Unpublished Class Notes. IT (AU), 1960.

3. Chalk, C. R. Additional Flight Evaluations of Various Longitudinal Handling Qualities in a Variable Stability Jet Fighter, Part II. Cornell Aeronautical Laboratory Report No. TB-1141-F-1. WADC, TR57-719, Part II, July 1958.

4. Bull, G. Minimum Flyable Longitudinal Handling Qualities of Airplanes. Cornell Aeronautical Laboratory Report No. TB-1313-F-1, December 1959.

5. Schuler, et al. Application and Evaluation of Certain Adaptive Control Techniques in Advanced Flight Vehicles, Second Quarterly Progress Report. Contract No. AF33(616)-7572. Cornell Aeronautical Laboratory Report No. 1D-1471-F-1, December 1960.

6. Boucher, R. and M. Marx. Navy Self Adaptive Control Flight Test Evaluation. Prepared under Bureau of Naval Weapons. Contract No. AS 59-6078C. Armament and Control Section LMED, General Electric, Schenectady, N. Y.

7. Campbell, G. Proposal for Research to Determine the Feasibility of the Use of an Adaptive Servo to Improve Airplane Flight Characteristics. Flight Research Memorandum, Cornell Aeronautical Laboratory, March 1955.

8. D'Azzo, John J., and Constantine H. Houpis. Control System Analysis and Synthesis. New York: McGraw-Hill Book Company, Inc., 1960.

9. Johnson, Clarence L. Analog Computer Techniques. New York: McGraw-Hill Book Company, Inc., 1956.

Appendix A

Sample Calculations for Root Locus Plots

In order to utilize standard Control System terminology the system block diagram as shown in Figure A-1 can be manipulated into that configuration shown in Figure A-2 as indicated below.

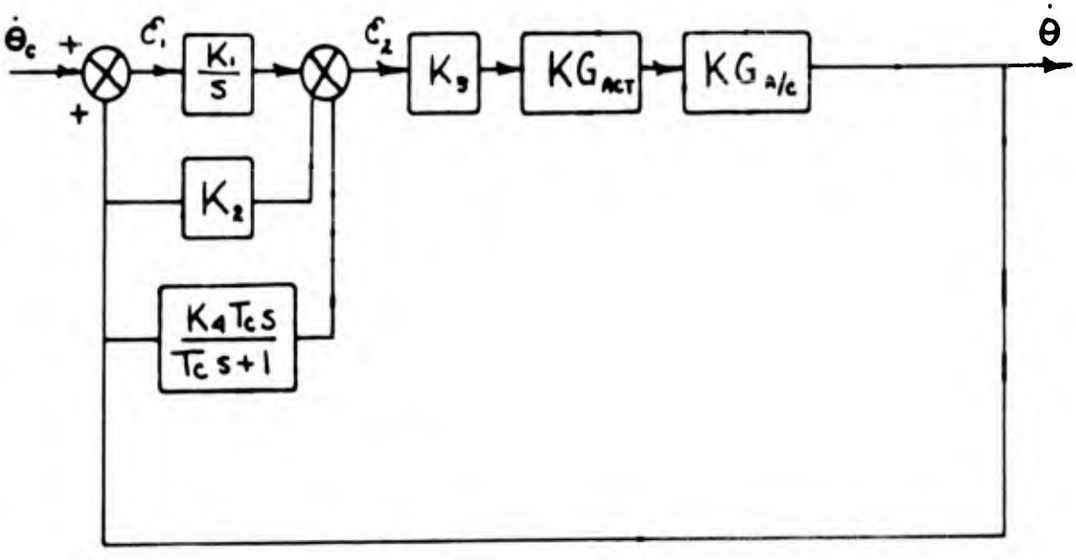

Fig. A-1 System Block Diagram

$$\mathcal{E}_2 = \mathcal{E}_1 \frac{K_1}{S} + \left(K_2 + \frac{K_4 T_c S}{T_c S+1}\right) \dot{\theta} \qquad \mathcal{E}_1 = \dot{\theta}_c - \dot{\theta}$$

$$\mathcal{E}_2 = \left(\dot{\theta}_c + \dot{\theta}\right) \frac{K_1}{S} + K_2 \dot{\theta} + \frac{K_4 T_c S}{T_c S+1} \dot{\theta}$$

$$\mathcal{E}_2 = \dot{\theta}_c \frac{K_1}{S} + \dot{\theta} \left[\frac{S^2 (K_4 T_c + K_2 T_c) + S (K_2 + K_1 T_c) + K_1}{S (T_c S+1)}\right]$$

The above equations indicate the transformation to Figure A-2.

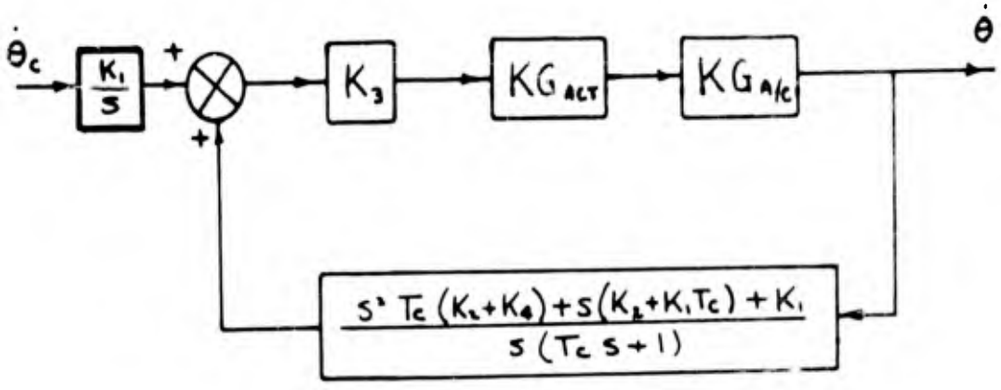

Fig. A-2 Block Diagram in Standard Form

From Reference 5 $KG_{ACT} = \frac{1000}{S^2 + 31.6S + 1000}$

and $K_1 = 1.0 \quad K_2 = 0.413 \quad K_4 = 3.39$

To derive the aircraft transfer function, the two basic equations of motion were solved simultaneously for $\frac{\dot{\theta}(s)}{\delta_e(s)}$ as indicated in Chapter IV

$$\frac{\dot{\theta}(s)}{\delta_e(s)} = \frac{s(M_\delta - L_\delta M_{\dot{\alpha}}) + (M_\delta L_\alpha - M_\alpha L_\delta)}{s^2 + s(L_\alpha - M_q - M_{\dot{\alpha}}) + (-M_\alpha - M_q L_\alpha)}$$

Using the data from Table A-1, page 56, the aircraft transfer function, evaluated for the t = 90 sec case is:

Table A-1

Numerical Data for X-15 Equations of Motion*

t sec	M_q	$M_{\dot{\alpha}}$	M_α	M_δ	L_α	L_δ
0	-.0011	-.0004	-0.1569	-.1131	.0016	.0002
20	-.002	-.0007	-0.3173	-0.2317	.0034	.0004
40	-.0078	-.0027	-1.5083	-1.1664	.0114	.0022
60	-.0595	-.0208	-11.11	-8.51	.112	.0172
74	-.1541	-.0539	-26.41	-17.5	.2795	.0417
90	-.1322	-.0463	-17.1	-12.2	.2767	.0372

* Adapted from Reference 5.

From Figure A-2 the forward loop transfer function becomes:

$$G(s) = \frac{1000\,K_3}{(s^2 + 31.6s + 1000)}\left(-\frac{12.2s + 2.75}{s^2 + 0.455s + 17.14}\right)$$

After substituting for K_1, K_2, and K_4 the transfer function in the feedback loop becomes:

$$H(s) = \frac{3.8(s^2 + 4.61s + 10.53)}{s(s + 40)}$$

Combining the above equations, with K_3 the variable gain, the open loop transfer function is obtained.

$$GH(s) = \frac{-K_3(1000)(12.2)(3.8)(s + 0.225)(s^2 + 4.61s + 10.53)}{s(s + 40)(s^2 + 31.6s + 1000)(s^2 + 0.455s + 17.14)}$$

or:

$$GH(s) = \frac{-46.4\ \ 10^3\ K_3\ (s + 0.225)(s + 2.3 \pm j\ 2.29)}{s(s + 40)(s + 15.8 \pm j\ 27.4)(s + 0.222 \pm j\ 4.14)}$$

The root locus of this open loop transfer function is shown in Figure 12. Similar computations were made for the other flight conditions.

Appendix B

Optimization Procedure for the Analog Simulation of the GESAC System

A systematic method which can be used to optimize the simulation as presented in this study is outlined below.

1. A root locus of the system (omitting the non-linear, gain changing loop) should first be drawn by plotting the open loop poles of the system characteristic equation. From this plot the variable gain (K_3) at the point where the system becomes unstable can be found for any given flight condition.

2. After wiring the computer circuit, the individual transfer functions should be checked by measuring the frequency or damping ratio from the uncontrolled response to a step input into the individual component.

3. The closed loop system, omitting the frequency sensor, is then checked by varying the gain K_3 (pot B-86) manually until the system output $\dot{\theta}$ just begins to oscillate. At this point the gain K_3 and the frequency of oscillation is measured from the computer trace and compared with the values obtained analytically from the root locus. If the computer circuit has been correctly set up, these values should match quite closely.

4. Next the frequency sensor loop is set up as shown in Figure D-1 with FSW B-2A in the UP position for calibration, and with the return from IG A-5 disconnected. This loop is now independent from the remainder of the system. Set pot A-84 at the input to the sine wave generator for the desired center frequency (ω_c = 35 radians/second) and calibrate the multivibrator by adjusting pot A-89 for zero output from IG A-3.

5. Calculate the approximate setting for the pot A-85, as shown under sample calculations in this appendix. Set remainder of pots in loop as specified in the list of pot settings.

6. To calibrate the output of the shaping network, offset the sine wave generator to 30 radians/second and adjust pot A-38 until the output of SU A-13 is + 40 v. Repeat this procedure for ω swg = 40 radians/second and check the output of SU A-13 for - 40 v.

7. Connect the output of IG A-5 into SU A-10 at the input to the sine wave generator and adjust pot B-87 until the ITAE output is minimized. (B-87 optimized at 0.4 for the t = 90 second case). With pot B-87 fixed now adjust feedback pot A-85 for minimum ITAE if necessary. Pot A-85 can now be optimized by adjusting for the best transient response of the output from IG A-3 (minimum settling time without excessive overshoot). The frequency sensor loop is now set for optimum transient response.

8. Disconnect the output from IG A-5 into SU A-10 and connect SU A-2 into servo 5. This disconnects the sine wave generator and connects the frequency sensor loop into the system. Next compute the setting for pot B-86 as shown under sample calculations. All other pot settings have been previously set as indicated. Now check system operation by measuring the system response to a step input $\dot{\theta}$ = 3 degrees/second. Any further refinements necessary can be made by readjusting pots B-86 or B-87 for minimum ITAE during a timed response to a step input.

9. For the above procedure note that the voltage out of IG A-5 represents the error signal for the ITAE, since this voltage represents the difference in frequency between the sine wave generator and the multivibrator.

Sample Calculations for Pot Settings A-85 and B-86

Pot B-86 at input actuator (refer to Figure D-1) should have a voltage output representing $K_3 \mathcal{E}_2$. From root locus calculations for the t = 90 seconds case at ω = 35 radians/second K_3 = .734.

Assume gain of SU A-6 = 5 and servo offset 25v, then

$$K_3 \mathcal{E}_2 = (B\text{-}86)\ (0.25)\ (5)\ \mathcal{E}_2 = 0.734\ \mathcal{E}_2$$

$$B\text{-}86 = \frac{0.734}{1.25} = 0.587$$

Calculations for setting pot A-85 are shown below. Refer to Figure 9 for wave-form and to Figure D-1 for computer schematic. Take maximum $\Delta\omega = 5$ radians/second

let $\omega_1 = 35$ radians/sec $\quad T = 0.179$

$\omega = 30$ radians/sec $\quad T = 0.209$

$\Delta T = 0.030$

$\frac{\Delta T}{2} = 0.015$ sec

Assuming the desired correction of the multivibrator half-period to be one third $\frac{\Delta T}{2}$, then compute the attenuation necessary so that the voltage out of pot A-85 when added to the output of IG A-11 will change the half period by 0.005 second.

The integration rate of IG A-11 = 279 volts/second

Volts needed from A-85 = (279) (0.005) = 1.39 volts

Volts into A-85 from IG A-3 = (750) (0.015) = 11.25 volts

Attenuation necessary = $\frac{1.39 \text{ volts}}{11.25 \text{ volts}} = 0.124$

Therefore the approximate setting for pot A-85 = 0.124

For the t = 90 sec case after optimization as described above, the setting for pot A-85 was 0.1265.

Appendix C

Sample Analog Computer Results

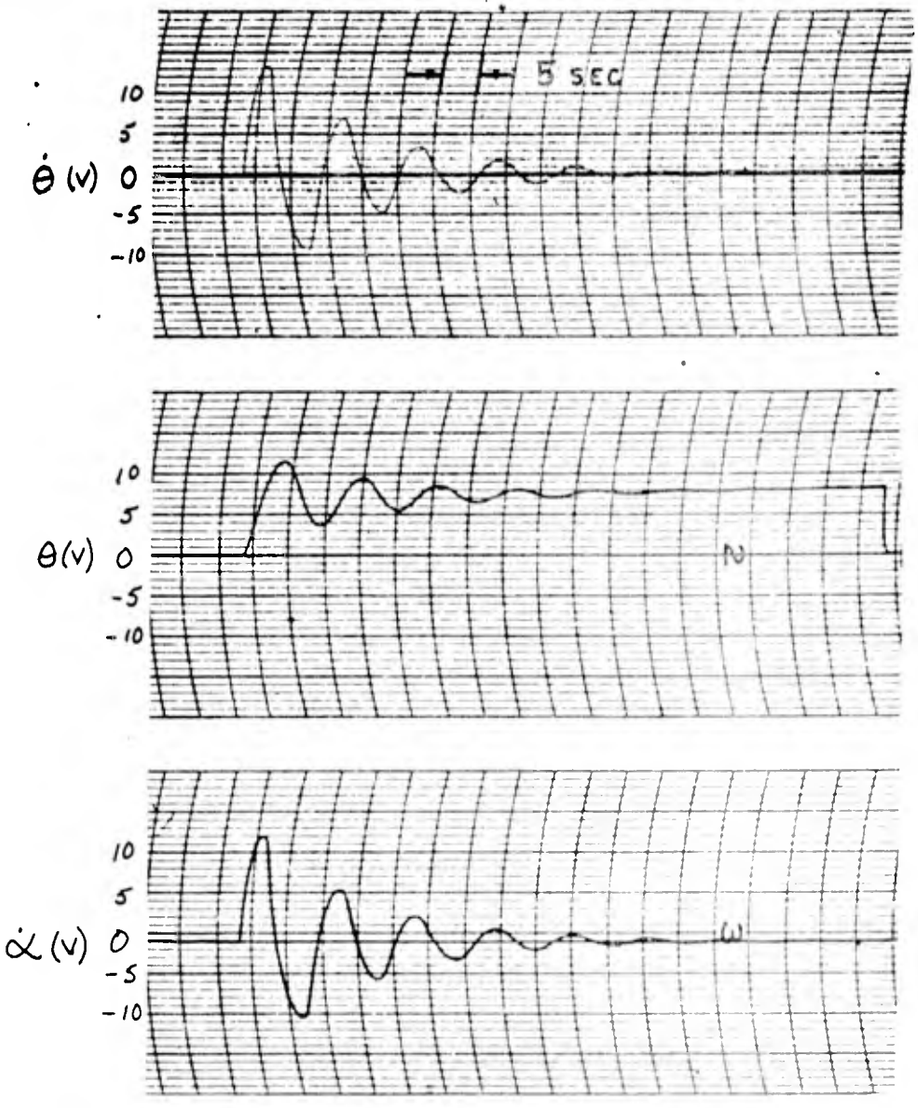

Fig. C-1 Uncontrolled Aircraft Response to θ Step Input (t = 40 sec)

From Calculations on above plot:

$\omega_{n\,a/c}$ = 1.24 radians/sec

ζ = 0.01

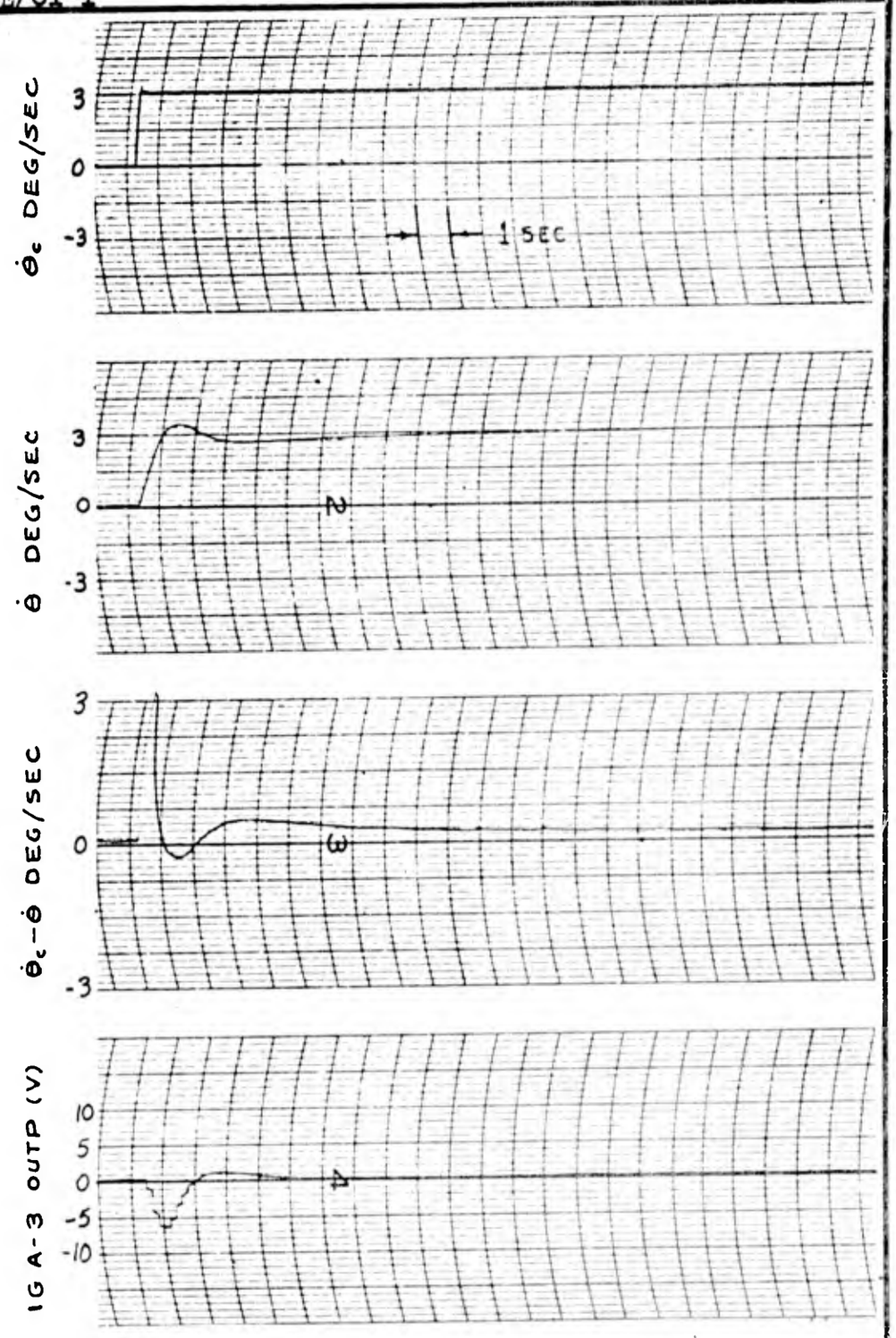

Fig. C-2 System Response to θ_c Step

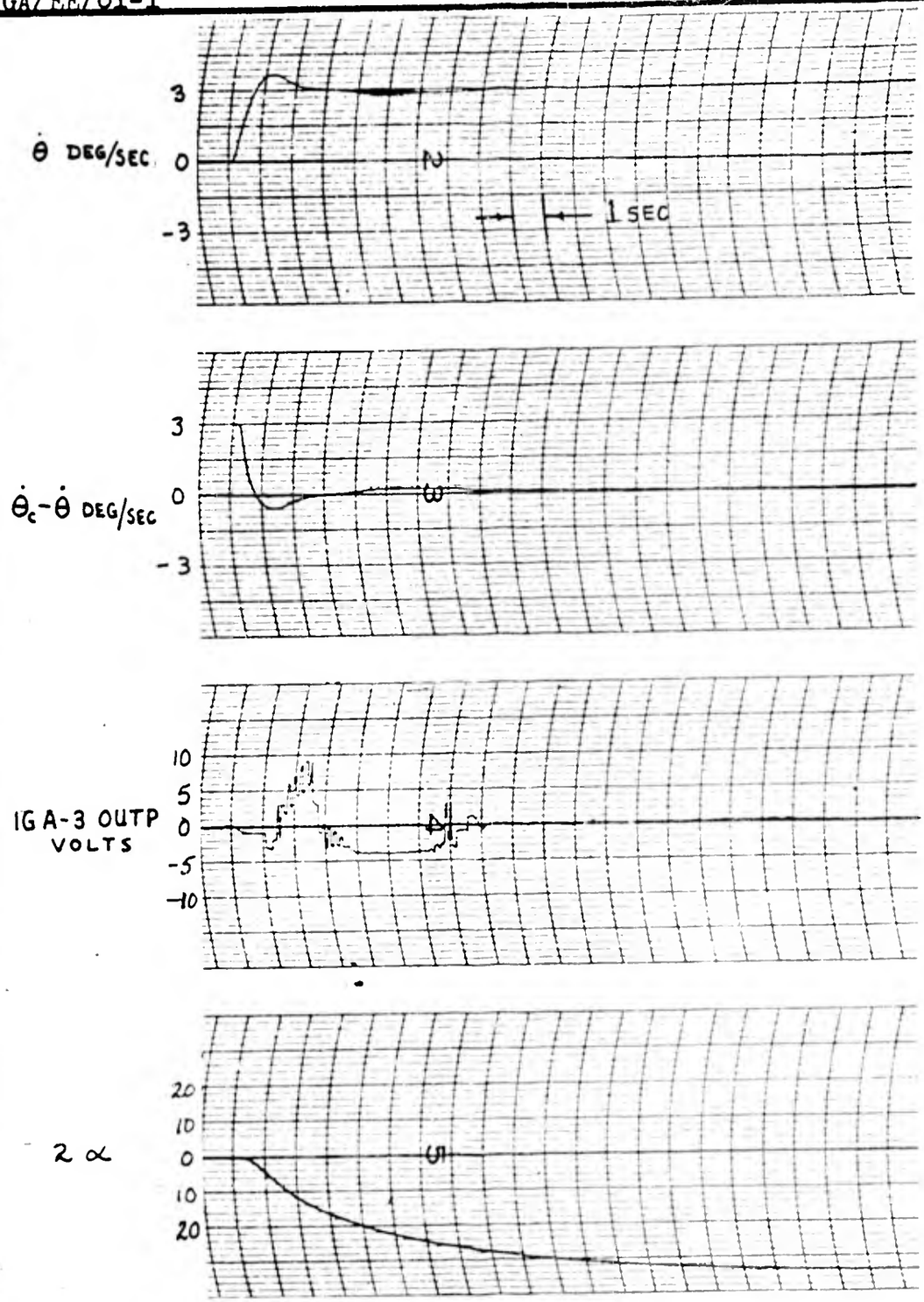

Fig. C-3 System Response to δ_e Step with High Gain (K_3) Setting

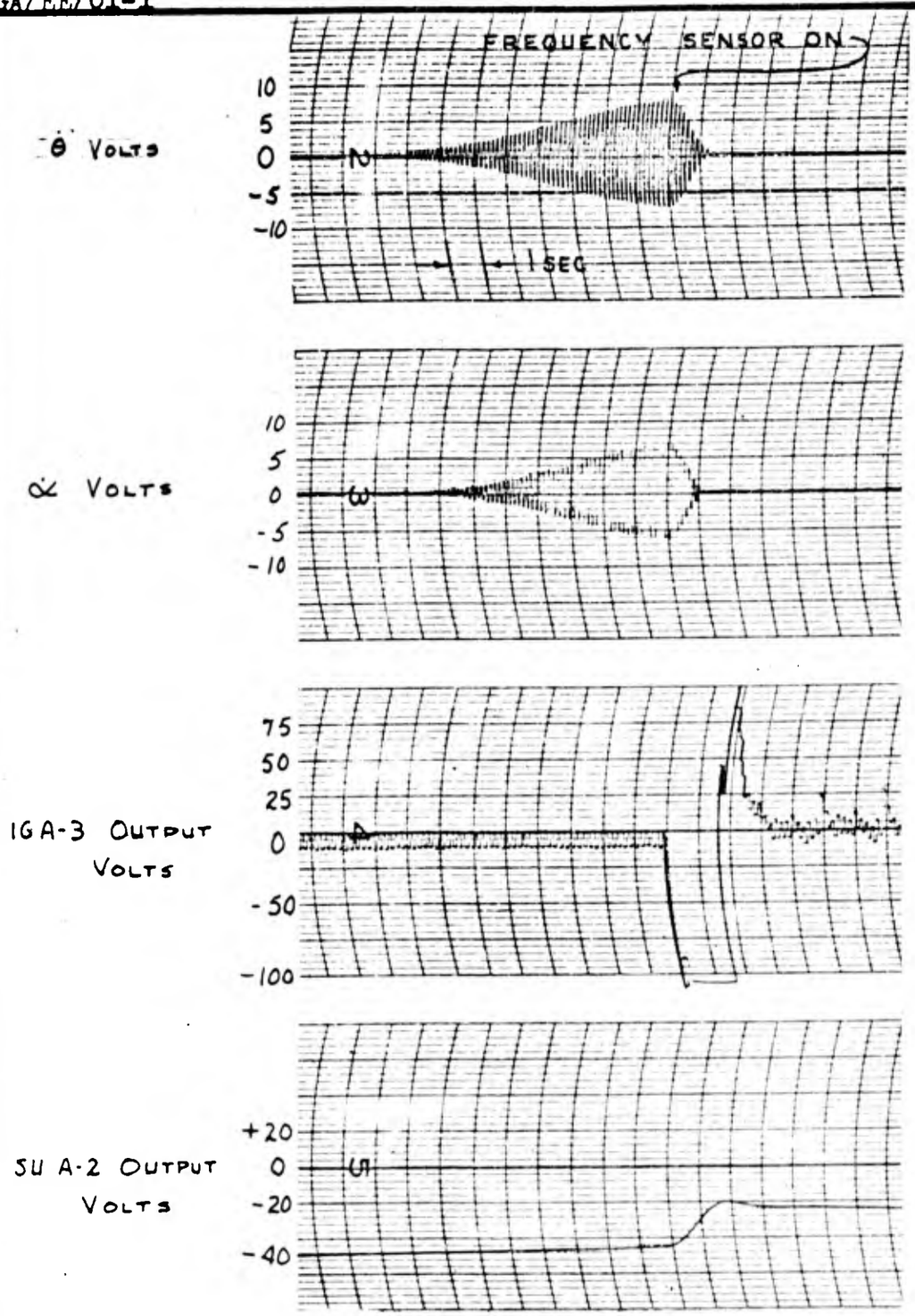

Fig. C-4 Recovery capability of Frequency Sensor Loop During System Instability

Appendix D

Complete Analog Schematic

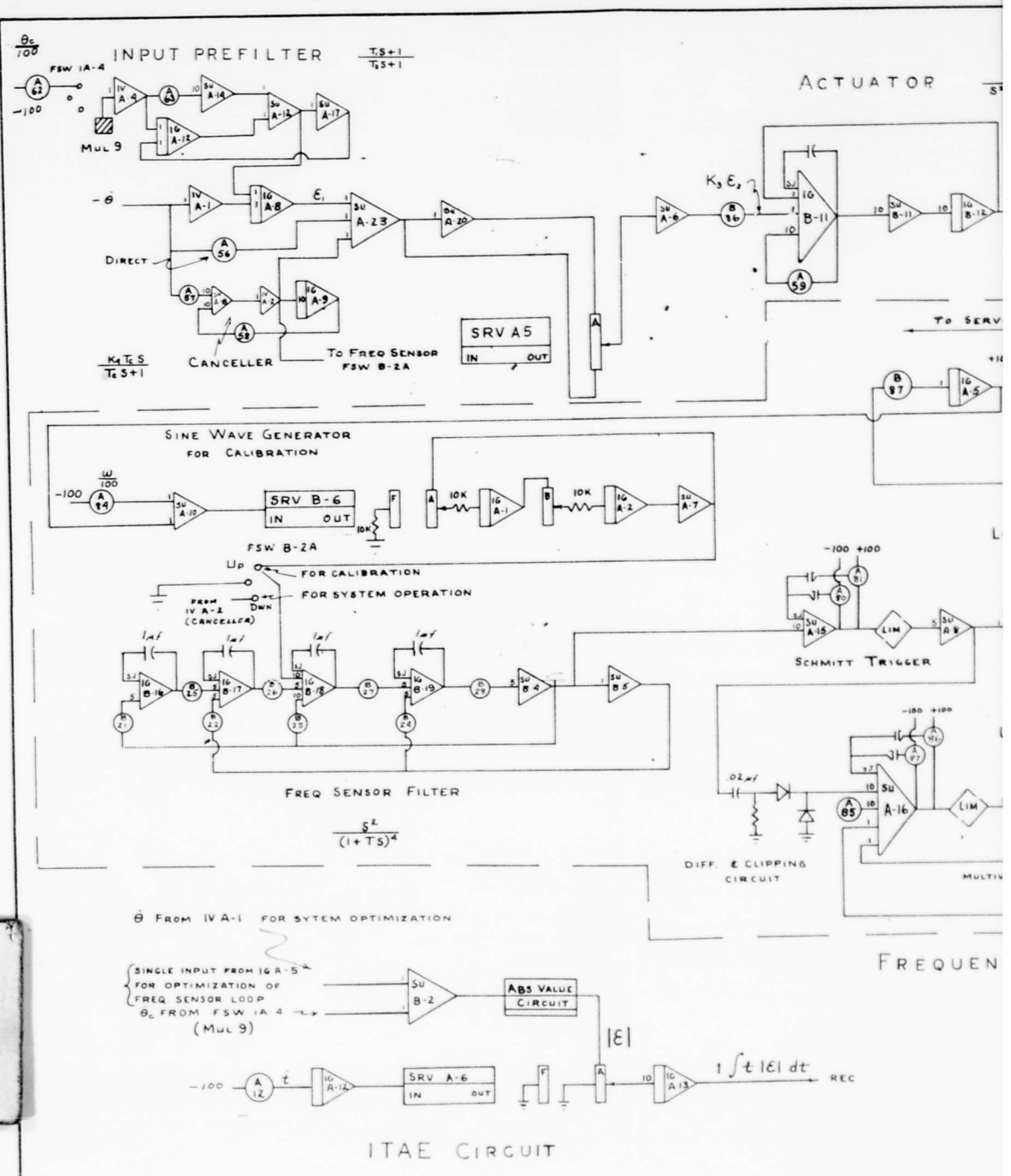

ITAE CIRCUIT

FIGURE D I COMPLETE ANALOG COMPU

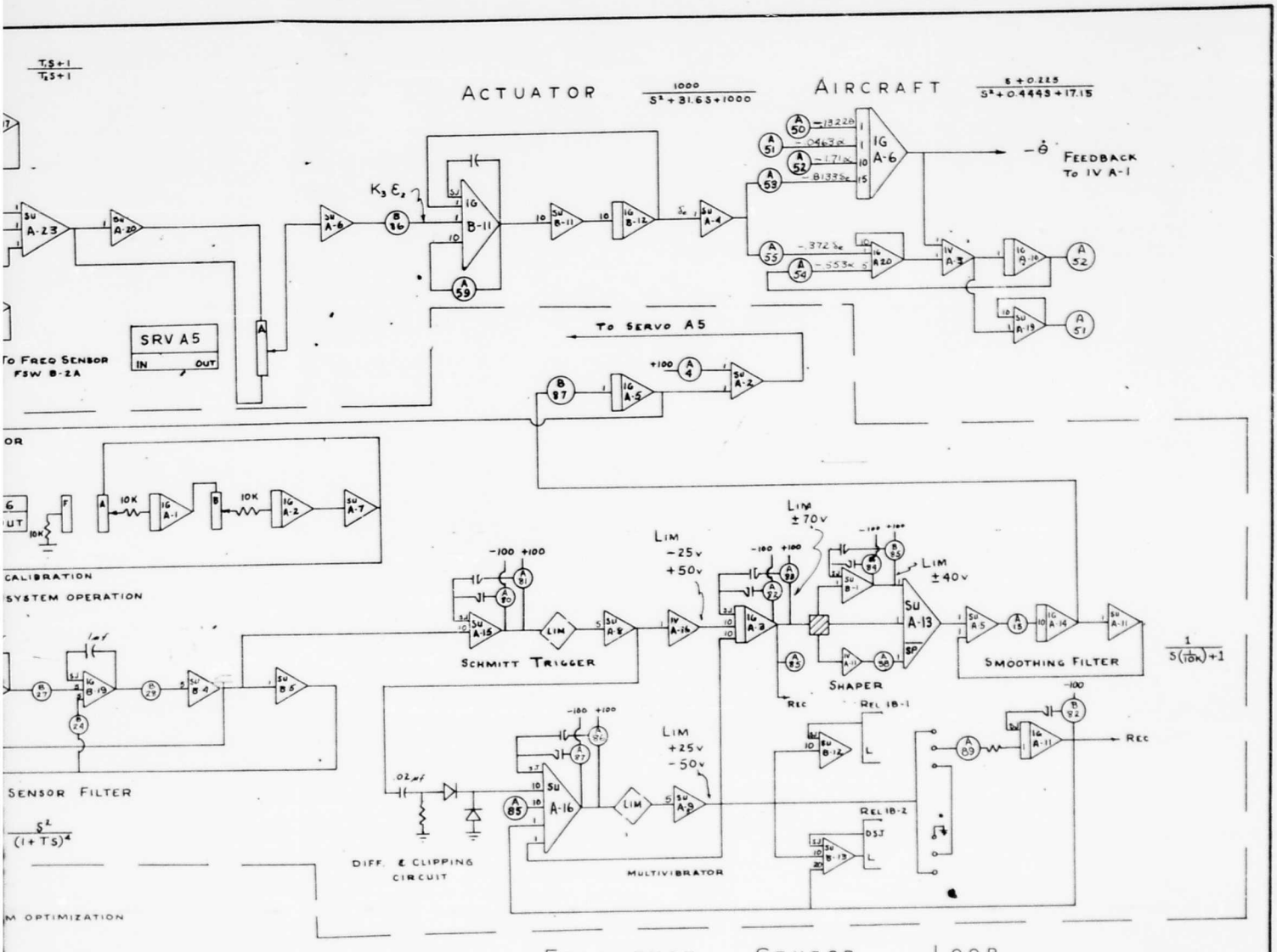

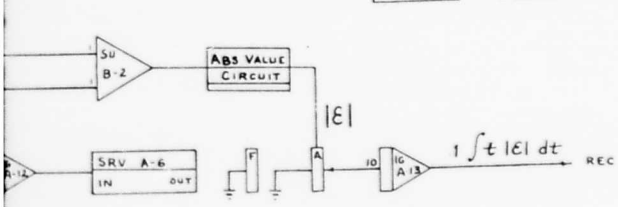

ITAE CIRCUIT

SYMBOLS

IG - INTEGRATOR
IV - INVERTER
SU - SUMMER
SRV - SERVO

2

FIGURE D1 COMPLETE ANALOG COMPUTER SCHEMATIC

Vita

Thomas John Deegan was born [redacted], [redacted]. He graduated from [redacted] High School in June 1943, at which time he enlisted in the Army as an Aviation Cadet. He received his commission as a navigator in 1944 and was assigned as a B-17 navigator-bombardier in Europe until 1945. In 1946 he entered the Air Force pilot training program, which he completed in 1948. He subsequently served two years as a fighter pilot before leaving the service in 1950. He was recalled to active duty in 1951, after completing two years of college work at Texas Western College, El Paso, Texas. In 1952 he was assigned to the Institute of Technology undergraduate program, from which he graduated in 1954 with a Bachelor of Science equivalent in Electrical Engineering. His last assignment prior to entering the Institute of Technology in 1959 was in ARDC, where he served with WADC as Chief of the Flight Test Radar Branch, in the Flight Test Engineering Division.

Permanent Address: [redacted]

This thesis was typed by Marjorie M. Keppler.